The evolution of a mid-crustal thermal aureole at Cerro Toro, Sierra de Famatina, NW Argentina

P.H. Alasino[1-2*], C. Casquet[3], M.A. Larrovere[1-2], R.J. Pankhurst[4], C. Galindo[3], J.A. Dahlquist[5], E.G. Baldo[5], C.W. Rapela[6]

[1] Centro Regional de Investigaciones Científicas y Transferencia Tecnológica de La Rioja (CRILAR-CONICET). Entre Ríos y Mendoza s/n, Anillaco (5301), La Rioja, Argentina
[2] INGeReN-CENIIT-UNLaR, Av. Gob. Vernet y Apostol Felipe, 5300, La Rioja, Argentina
[3] Depto. de Petrología y Geoquímica – IGEO (Universidad Complutense, CSIC), 28040 Madrid, Spain
[4] British Geological Survey, Keyworth, Nottingham NG12 5GG, United Kingdom
[5] CICTERRA-CONICET-UNC, Av. Vélez Sarsfield 1611, Pab. Geol., X5016CGA-Córdoba, Argentina
[6] CIG-CONICET-UNLP, Calle 1 No. 644, 1900, La Plata, Argentina

[*]*Corresponding author.*
E-mail address: palasino@crilar-conicet.gob.ar

Abstract

A more than 12 km wide sheeted tonalite complex in western Sierra de Famatina, NW Argentina, was emplaced at middle crust levels (ca 5 kbar), coeval with regional metamorphism during an early phase of the Ordovician Famatinian orogeny (ca. 480 Ma). Advective heat from the tonalite complex caused a rise in the host regional temperatures (≤ 700ºC) by a maximum of ca. 100ºC, developing an aureole (~3 km wide) parallel to the igneous contact. This was accompanied by significant melting (ca 40 %) of the host rocks that hybridized to a variable extent with the tonalitic magmas. Three metamorphic zones were distinguished in a cross-section through the aureole: (1) an external zone consisting of metatexitic gneisses, amphibolites and minor tonalites, (2) an intermediate zone formed by screens of highly melted gneisses, amphibolites and metagabbros lying between tonalite and newly formed leucogranitoid and hybrid rock sheets, (3) an internal zone formed almost exclusively of massive tonalite and minor hybrid rocks. Incongruent melting of biotite in gneisses of the intermediate zone produced peritectic cordierite and garnet. Hybrids resulting from variable mixing of anatectic granitoids and tonalite magma developed in the innermost part of the aureole at 750-800ºC. Increased water activity within this zone eventually promoted increased melting of plagioclase + quartz in the gneisses. Leucogranitoid magmas formed in part by extraction from the hybrid magmas led to heterogeneity of the Sr-isotope composition. The Cerro Toro contact aureole shows that assimilation of metasedimentary rocks through partial melting can play an important role during emplacement of tonalitic magmas at mid-crustal levels.

Keywords
Aureole; Anatexis; I-type magmatism, Hybridization; Isotopic disequilibrium; Sierra de Famatina

1. Introduction

Thermal aureoles induced by advection of magmas are an excellent natural laboratory for the study the wall-rock magma interaction processes (e.g., Paterson et al., 1991; Paterson and Farris, 2008 and references therein). Classical examples of thermal aureoles occur when hot magmas intrude upper crustal levels, causing contact metamorphism due to the high thermal contrast between magma and wall-rock. These effects are rather well understood today after long research following the first recognition of contact metamorphism in the late 18th century by James Hutton (e.g., Rastall, 1910; Kerrick, 1970;

Pattison and Harte, 1985, among many others). However, mid-crustal thermal aureoles show greater complexity, due to reduced thermal contrast between magma and the host rocks (which are often affected by pre- or syn-regional metamorphism). In contrast with epizonal contact metamorphism, slow cooling (e.g., Nabelek et al., 2012) permits processes such as assimilation, mingling, mixing and partial melting of the country rocks, (e.g., Yardley and Barber, 1991; Ugidos and Recio, 1993; Finger and Clemens, 1995; Greenfield et al., 1996; Jung et al., 1999; Barnes et al., 2002; Harris et al., 2003; Saito et al., 2007). When assimilation occurs its chemical effects are often recognizable, but the physical processes that caused them are less obvious (e.g., Clarke, 2007; Erdmann et al., 2009).

A new example of a contact thermal aureole at mid-crustal level is described from Cerro Toro, in the western Sierra de Famatina (Sierras Pampeanas, NW Argentina, see Fig. 1a). Here, at paleodepths of ca. 17 km, voluminous metaluminous magmas formed a huge sheeted complex (ca 12 km wide) in predominantly metasedimentary country rocks. A 3-km wide hybridization zone is well displayed along the contact, containing many screens and stoped blocks of host rocks. Although conceptual models of hybridization have recently been well established (e.g., Beard et al., 2005; Beard, 2008), many questions still remain open concerning natural examples of large-scale interaction between partially molten country-rocks and metaluminous magmas, such as the processes of formation of hybrids and melt extraction during the anatexis. We describe the sheeted intrusions at Cerro Toro, their contact relationships with host-rock screens and stoped blocks, and the partial melting and hybridization processes that occurred in the aureole. We also emphasize the mechanisms that might occur in a regional thermal aureole at mid-crustal level as part of the general construction of magma chambers in orogenic belts.

2. Regional setting

The proto-Andean and subsequent Andean margin of Gondwana has been active from at least the Early Ordovician until the present, which has led to the generation of huge volumes of plutonic and volcanic rocks of different ages. Part of this history is well exposed in the Sierras Pampeanas of NW Argentina (20° - 40°S), exposed by tilting of the rigid basement blocks in the Miocene during Andean compression (e.g., Jordan and Allmendinger, 1986). Geochronological data show that four main Paleozoic episodes of granitic magmatism took place in the Sierras Pampeanas: a) Early Cambrian (Pampean orogeny), b) Early–Middle Ordovician (Famatinian orogeny), c) Middle–Late Devonian (Achalian orogeny) and d)

Early Carboniferous. The Famatinian orogeny overprinted the pre-Ordovician terranes along the southwestern Gondwana margin between present Patagonia and Venezuela (Cawood, 2005) and resulted in abundant magmatism in the Sierras Pampeanas (e.g., Pankhurst et al., 1998). The Famatinian Cerro Toro sheeted-complex is found in the western Sierra de Famatina (Fig. 1a), from which the name of the orogeny was derived.

Pankhurst et al. (2000) recognized three distinct Famatinian granitoid-associations in the Sierras Pampeanas: 1) voluminous I-type, 2) more restricted S-type, and 3) minor tonalite–trondhjemite–granodiorite (TTG) type, all emplaced within the interval 484–463 Ma. Detailed petrological, geochemical and isotope studies were carried out by Rapela et al. (1990), Saavedra et al. (1998), Pankhurst et al. (1998, 2000), Dahlquist and Galindo (2004), Miller and Söllner (2005), Dahlquist et al. (2008, 2013), Ducea et al. (2010), Otamendi et al. (2009, 2012), and Castro et al. (2013), among others. I-type intrusions range from gabbro to monzogranite but tonalite and granodiorite are largely dominant. εNd_t values range from −3 to −9. Only a few Famatinian igneous rocks have positive values of εNd_t between +0.2 to +4.8 (Pankhurst et al., 2000, Otamendi et al., 2009, 2012; Casquet et al., 2012).

3. Sierra de Famatina

The Sierra de Famatina in north-western La Rioja province shows well-exposed sections across the transition from mid-crustal levels in the west (metaluminous basic to intermediate plutonic rocks hosted by gneiss, migmatite, amphibolite and minor meta-basic rocks) to shallow levels in the centre and the east (acidic plutonic and volcanic rocks and low- to very low-grade phyllite, metapsammite and chert). Previous geochronological data from the western Sierra de Famatina yielded Early–Middle Ordovician ages (Pankhurst et al., 2000; Dahlquist et al., 2008). We focus here on an area on the western slope of the Sierra de Famatina, near Villa Castelli (Figs. 1a and b). This area is mountainous (up to 2000 metres a.s.l.) and consists from west to east of several sierras: Cerro Asperecito, Cerro Toro, and the northern end of Cerro La Puntilla (Fig. 1b). Here, we recognize the Cerro Toro igneous complex (Toselli et al., 1988; Saavedra et al., 1992, 1996) consisting of a succession of steeply-dipping sheets of tonalite and a large inner pluton that strikes ~N–S and is about 25 km wide (Fig. 1b). The steep dip is probably a primary feature as suggested, for example, by near-vertical strings of stoped blocks within the sheets (see also Castro et al., 2008). Host rocks to the sheets are high-grade metamorphic rocks that display from west to east an increase in grade from amphibolite to granulite facies. Metamorphic rocks are found as screens and stoped blocks within the igneous complex and altogether constitute a medium-P/high-T regional thermal aureole, i.e., the Cerro Toro thermal aureole. Emplacement at relatively deep crustal levels and under conditions close to anatexis was previously suggested by Saavedra et al. (1992).

4. The Cerro Toro thermal aureole

Three zones can be recognized within the aureole on the basis of field relations, lithology, mineralogy and modal composition. They are well displayed in W-E section: (i) *external,* with high-grade metamorphic rocks, and sheeted bodies of metaluminous igneous rocks (in part of the zone only) and late peraluminous granitoids, (ii) *intermediate,* heterogeneous, with high-grade, partially melted, metamorphic rocks and evidence of widespread hybridization with metaluminous magmas, and (iii) *internal*, consisting mostly of a large tonalite pluton, that extends about 25 km to the east (see Fig. 1b, Table 1 and Supplementary data). Although there is no continuity between the external and the intermediate zones because of disruption by Andean faulting, field relationships and thermobarometry data show that they were parts of the aureole at similar depths. Emplacement of metaluminous magmas and regional metamorphism were largely coeval, which is a distinctive feature of the Famatinian orogeny (e.g., Dahlquist et al., 2005; Ducea et al., 2010; Otamendi et al., 2012, Casquet et al., 2012). U-Pb SHRIMP zircon dating of a hybrid rock from the intermediate zone (FAM7086) has yielded an age of 481 ± 4 Ma with a low zircon εHf_t typical of a crustal component (Dahlquist et al., 2008, 2013). We consider that this age corresponds to the emplacement of the Cerro Toro complex.

4.1. Description of the zones forming the thermal aureole

4.1.1. External zone

This zone consists mainly of high-grade metamorphic rocks, metatexites with minor intercalations of gneisses, and amphibolites, and is exposed at Cerro Asperecito (Fig. 1b). Foliation is NNW-SSE and dips steeply to the north. Metatexitic gneisses display a stromatic structure with alternating biotite-rich mesosome, quartz-feldspathic leucosome and biotite and fibrolite-rich melanosome (Fig. 2a). Amphibolites are lens-shaped or tabular and resulted from transposition and metamorphism of former basaltic dykes. On the north-eastern side of Cerro Asperecito (Fig. 1b) metatexitic gneisses and amphibolites are intercalated with sheets of Bt±Hbl tonalite and lesser granodiorite of the Cerro Toro igneous complex, largely concordant to the external foliation (sheets, < 1 km wide). Most of these bodies show magmatic foliation. Mafic microgranular enclaves, schlieren and xenoliths are common. Mafic intrusions are scarce either as < 15 m wide dykes of gabbro-diorite or as small amphibole gabbro bodies. Peraluminous granites (e.g., Peñón Rosado pluton) containing magmatic garnet and muscovite crop out here (Fig. 1b) but they are younger (469 ± 4 Ma, Dahlquist et al., 2007) than the metaluminous intrusions (Fig. 1b).

4.1.2. Intermediate zone

This is located on the western flank of Cerro Toro (Fig. 1b). It is ca. 3 km wide and heterogeneous, displaying a gradual transition from migmatite, through hybrid to leucogranitoid, together with tonalite sheets. Hybrid rocks predominate; they are formed by mixing of the tonalitic magma with partially molten metasedimentary rocks exhibiting a ~N-S sheeted structure. From W to E, they gradually lose the relict metamorphic foliation (defined by biotite) and gradually pass into leucogranitoids. This zone also contains screens and stoped blocks of migmatites, amphibolite and metagabbro up to 3 km long all aligned parallel to the structures in the external zone (Figs. 1b and 3a). Many of these refractory blocks (i.e., amphibolite and metagabbro) are engulfed by leucogranitoids (Fig. 3b), mostly with sharp contacts. Because both screens and blocks resulted from continuous dismemberment at different scales, we will hereafter use block to refer to both. Leucogranitoids in this zone (Table 1 and Fig. 2b) are of two types, (i) leucogranitic or (ii) leucotonalitic. They can be found enveloping migmatite blocks or as concordant or discordant bodies of variable thickness that intruded hybrid and tonalite rocks. Two magmatic foliations can be recognized: ~ N-S and W-E. Contacts between all these rocks can be irregular, and gradational or sharp (Figs. 3c, d and e), implying that peak metamorphism, tonalite intrusion and partial melting were almost contemporaneous. Mafic microgranular enclaves, xenoliths and schlieren are common to all these rocks.

On a W-E cross-section through the intermediate zone three domains can be distinguished based on the predominance of specific rock-types (Fig. 1b): (1) Domain-I. *Bt-Sill±Crd migmatites* (Table 1). Migmatite blocks here are diatexites, often with schlieren structures (terms after Sawyer, 2008) formed by diffuse quartz-feldspar rich bands and thinner and more discontinuous biotite ± cordierite-rich layers, defining a coarse foliation (Fig. 2c). The more homogenous diatexite migmatites are found as patches within and at the outer boundaries of the large migmatitic blocks, the cores of which sometimes exhibit a gneissic texture. (2) Domain-II. *Bt-Sill±Grt±Crd migmatites* (Table 1): this domain is defined by the sudden appearance of garnet, together with a modal increase of cordierite in the blocks. Their size decreases significantly (< 1.2 km in length) (Fig. 1b). Texturally, migmatites tend to be more homogenous (e.g., FAM143, Fig. 2d). (3) Domain-III. *Bt±Amp±Cpx±Kfs hybrid rocks* (Table 1; Fig. 1b): this is characterized by the predominance of hybrid rocks, leucogranitoids and tonalites. Hybrid rocks commonly show a massive texture but they contain recognizable metamorphic phases (e.g., biotite-2, see § 6.2). Interpretation of the hybrids as mixtures of partially molten metasedimentary rocks (anatectic melt ± residuum) and tonalitic magma is supported by the low εHf_t value (-14.7) of zircon from a sample of this zone (FAM7086, Dahlquist et al., 2013).

4.1.3. Internal zone

This is the easternmost zone and encompasses the eastern flank of Cerro Toro and the northern part of Cerro La Puntilla (Fig. 1b). Here the main rock type is tonalite with a NNW-SSE magmatic foliation defined by orientated biotite and hornblende and containing many mafic microgranular enclaves and some stoped blocks of amphibolite or metagabbro. At the contact with the intermediate zone, leucogranitoids intruded the solidified tonalite front (Fig. 3f). In comparison with the hybrids of the intermediate zone with biotite-2, the hybrid rocks here (Table 1) show a greater proportion of tonalite-derived component such as biotite-4 (see § 6.2) and hornblende. Contact relationships between hybrid and tonalite have not been observed.

In summary, I-type tonalite intrusions were emplaced into heterogeneous rocks (mainly, metasedimentary) affected by coeval regional metamorphism. With increasing proximity to the main tonalite pluton a gradual transition is recognized from metatexitic gneisses (external zone), through diatexite to hybrid and leucogranitoid (intermediate zone). Hybrid and leucogranitic rocks are the result of the interaction between anatectic (±solid phases) and I-type magmas. A scheme intended to summarize the relationships between rocks and processes within the aureole is shown in Figure 4.

5. Analytical methods

Petrographic investigations were conducted on more than 120 representative samples, of which 31 were selected for major and trace element whole-rock analysis using ICP-OES, ICP-MS and/or INAA at ACTLABS, Canada following the procedures described as 4-Lithoresearch and 4E-research codes (methods in www.actlabs.com). Additionally, three representative igneous samples were analysed by

GeoAnalytical Lab, Washington State University, using a ThermoARL sequential X-ray fluorescence spectrometer, following the procedure described by Johnson et al. (1999). All geochemical data are listed in Table 2. Twelve whole-rock analyses published by Dahlquist et al. (2007, 2008) also have been used. Sr and Nd isotope analysis of fourteen representative samples was carried out at the Geochronology and Isotope Geochemistry Center, Complutense University (Madrid, Spain) using an automated multicollector VG® SECTOR 54 mass spectrometer. Errors are quoted throughout as two standard deviations from measured or calculated values. Analytical uncertainties are estimated to be 0.006% for $^{143}Nd/^{144}Nd$ and 0.1% $^{147}Sm/^{144}Nd$, the latter parameter determined by isotope dilution. Fifty-six analyses of La Jolla Nd-standard over one year gave a mean $^{143}Nd/^{144}Nd$ ratio of 0.511846±0.00003. Additionally, ten Sr and Nd isotope analyses were taken from Dahlquist and Galindo (2004) and Dahlquist et al. (2008). Mineral compositions were determined using a JEOL Superprobe JXA-8900-M equipped with five crystal spectrometers at the Luis Brú Electron Microscopy Center, Complutense University, Madrid, Spain. Operating conditions were: acceleration voltage 15 kV, probe current 20 nA, beam diameter 1– 2 µm. Absolute abundances for each element were determined by comparison with mineral standards (Jarosewich et al., 1980; McGuire et al., 1992), using an on-line ZAF programme.

6. Petrography and mineral chemistry

6.1. Texture and mineral assemblages

6.1.1. Migmatites

Migmatites from the external zone (metatexitic gneisses) consist of Qtz + Pl + Bt_1 ± Sill (Fib) (Table 1 and Supplementary data) (for the biotite numbers see section § 6.2). As in the intermediate zone, migmatites here show evidence of a melt-phase as suggested by igneous textures such as crystal faces of plagioclase against quartz typical of crystallization from a melt (Vernon, 2004). The mineral assemblage of migmatites from domain I of the intermediate zone is Qtz + Pl + Crd + Bt_1 ± Sill (Fib) ± Kfs. That for migmatites in domain II is Qtz + Pl + Crd + Grt + Bt_2 ± Sill (Fib) ± Kfs. Cordierite (0.56 > X_{Mg} > 0.61, see Supplementary data), increases from 4 to 11 vol. % on going from domain I to II and occurs either as orientated medium-grained crystals (often altered to muscovite) or large (up to 4 x 2 cm) prismatic euhedral crystals that include biotite and fibrolite (Fig. 5a). The latter type of cordierite can be found cross-cutting the quartz-feldspathic layers of diatexite (Fig. 2c). Garnet ($Alm_{71\text{-}74}$-$Grs_{3\text{-}4}$-$Prp_{10\text{-}14}$-$Sps_{8\text{-}16}$) only exists in domain II migmatites (up to 3.5 vol. %) and is found as subhedral crystals up to 2.5 cm in size (Fig. 2d). Compositionally, it shows a flat zoning pattern with a slight increase in spessartine content from core to rim (see Supplementary data). Late muscovite is common in both external and intermediate zones; it is a retrograde mineral that grew late relative to foliation development.

6.1.2. Tonalites

The typical tonalite consists of plagioclase (An_{48-53}) + quartz + biotite-4 + hornblende, and shows a magmatic hypidiomorphic-granular texture. Close to the boundary with the intermediate zone tonalite of the main pluton exhibits sericitization, and epidotization of plagioclase cores and hornblende, and chloritization of biotite. Secondary epidote can be up to 10 modal %.

6.1.3. Hybrid rocks

Hybrid rocks of the intermediate zone consist of plagioclase + quartz + biotite-2 as essential minerals. Plagioclase exhibits anhedral to subhedral forms with skeletal (box-like-cellular - Fig. 5b) or dusty cores sometimes surrounded by albitic rims (An_{33}). The skeletal plagioclase core is An_{39-43} in composition – intermediate between that of tonalite (An_{49-53}) and metamorphic plagioclase (An_{15-36}). Biotite shows a modal variation (from 20 to 10 %, see supplementary data and Fig. 1b) on going from domain II to III. Clinopyroxene appears as isolated subhedral to euhedral crystals only in domain III. Amphibole occurs either as anhedral crystals including rounded relics of plagioclase, quartz and biotite-2 (Fig. 5c) or replacing clinopyroxene along its boundaries with plagioclase. On the other hand, hybrid from the main pluton (sample FAM212, internal zone) is formed by plagioclase + K-feldspar + quartz + biotite-4 + hornblende. Plagioclase core composition is An_{37-45} surrounded by more albitic rims (An_{24-30}). Hornblende forms subhedral to euhedral crystals.

6.1.4. Leucogranitoids

Leucogranitoids of the intermediate zone range from leucotonalitic to leucogranitic (Table 1). Sometimes this modal mineral variation occurs in the same igneous body. Examples of plagioclase-rich rocks (leucotonalite samples FAM326, 398, 399) show variations from a mineral association consisting of anhedral to subhedral plagioclase (An_{17-42}), biotite-2 and recrystallized quartz to one of monomineralic plagioclase, sometimes showing triple points (Fig. 5d). K-feldspar is scarce (< 1 %) and appears in thin films between recrystallized quartz and plagioclase grains or occupying the volume after partially dissolved plagioclase (Figs. 5e). Conversely, leucogranites (e.g., FAM397) show typical granitic texture consisting of Ab-rich plagioclase (An_{11-25}, with tabular forms), microcline and biotite-3 (Fig. 5f). K-feldspar is interstitial or forms well defined medium- to coarse-grained crystals. Some rocks (e.g. FAM333, 399) have petrographic characteristics common to both types of leucogranitoids. In thin-section, these rocks exhibit K-feldspar rich zone in contact with monomineralic plagioclase domain, the former consisting of coarse-grained microcline with inclusion of plagioclase (An_{18-33}; crystals devoid of inclusions and with convex boundaries, Fig. 5g). Epidote and titanite can found associated with or included in K-feldspar (Fig. 5h).

Chemical zoning of plagioclase is common in the leucogranitoids. Zoning patterns however are remarkably diverse: (1) An-rich cores (An_{37-43}) surrounded by more albitic rims (An_{26-35}); (2) Ab-rich interiors (An_{18-21}), surrounded by a zone richer in anorthite (An_{30-36}); (3) slightly zoned crystal (An_{27-33}) surrounded by more albitic rims (An_{18-24}) and (4) tabular plagioclase (An_{11-25}) with normal zoning (Fig. 5f). Types 1, 2 and 3 can be recognized in the same thin-section.

6.2. Biotite textural and compositional variation

The petrographic description above of rocks across the aureole shows that biotite is a major phase in all the samples. The chemical composition and texture of biotite characterize the different lithological units in the aureole. Four main groups of biotite have been recognized (Fig. 6 and Supplementary data): (1) Biotite-1 occurs in metatexite migmatites (FAM349) from the external zone, and in Crd-bearing diatexite blocks (FAM135 and 408) corresponding to domain-I (intermediate zone). It is fine to medium-grained, subhedral to anhedral. Common inclusions are monazite, zircon, Ti-magnetite and apatite. Chemically, biotite-1 (n = 20) has X_{Fe} [=Fe/(Fe+Mg)] values between 0.42 and 0.47, intermediate Ti content (from 0.18 to 0.26 a.p.f.u.) and low Mn (from 0.03 to 0.09 a.p.f.u.). Biotite-1 is taken to have formed during regional metamorphism immediately preceding emplacement of the tonalite. (2) Biotite-2 occurs in Grt-Crd bearing diatexite blocks (FAM143 and 339), leucogranitoids (e.g., FAM333 and FAM346) and hybrid granitoids (FAM7086,) of intermediate zone domains II and III. Biotite-2 commonly shows inclusion patterns similar to biotite-1. However a marked pleochroism from light to dark brown or even reddish hues, and sometimes rounded shapes are common. Biotite-2 shows higher and more variable values of X_{Fe} (from 0.55 to 0.62), Ti (from 0.20 to 0.40 a.p.f.u.) and Mn (from 0.01 to 0.17 a.p.f.u.) (n=37). Biotite-2 in migmatite reflects increasing metamorphic grade towards the contact with the main igneous body (internal zone). Biotite-2 in leucogranitoid/hybrid rocks is probably a residual mineral from anatexis. (3) Biotite-3 is present in some leucogranitoids of the intermediate zone (FAM397). In contrast biotite-3 is fine-grained, euhedral to subhedral and pleochroic with minor inclusions. It yields high X_{Fe} values between 0.64 and 0.69, and a wide range of Ti contents (0.22 to 0.42 a.p.f.u) and more restricted Mn (0.06 to 0.12 a.p.f.u.) (n=8). Biotite-3 commonly occurs as isolated crystals or small clusters suggesting a magmatic origin (Sawyer, 1999). (4) Biotite-4 is hosted in amphibole-bearing tonalites (ASP120) from the external zone and in hybrid rocks from the internal pluton of the aureole (FAM212). Biotite-4 occurs as medium-grained, euhedral and pleochroic crystals with small inclusions of zircon, monazite and apatite. It has intermediate X_{Fe} values (from 0.49 to 0.52), high Ti (from 0.30 to 0.37 a.p.f.u.) and low Mn (from 0.04 to 0.07 a.p.f.u.) (n=5) making it easily distinguishable from the other biotites. Biotite-4 is interpreted as magmatic.

7. Metamorphism

7.1. Prograde mineral reactions

The absence of muscovite as a prograde mineral, which should be expected from the shale/wacke protolith of the migmatites, implies that this mica was consumed in lower-grade metamorphic zones (not visible) by reactions such as Chl + Ms = Als + Bt + V (R1) (Spear and Cheney, 1989), followed by water saturated reactions of the type Ms + Pl + Qtz + V = Als + Kfs + melt (R2) and Ms + Pl + Qtz + V = melt (R3) [melting reactions (R2) throughout (R5) are from Spear et al. (1999); for P-T conditions see below]. The latter two reactions that consume muscovite and produce (hydrous) melt, probably led to the metatexites of the external zone. The modal decrease of biotite and the occurrence of cordierite and garnet with increasing grade (intermediate zone) suggests that biotite dehydration melting also played a role through reactions R4 and R5 (see below). Evidence for melting in the intermediate zone diatexites is provided by textures such as feldspars and cordierite showing crystal faces against quartz, simple twinning in K-feldspar, and aligned euhedral cordierite crystals (e.g., Vernon, 2011). Cordierite encloses foliation-forming biotite and fibrolite (Fig. 5a) implying that the latter minerals were partially dissolved when cordierite formed. Thus, a peritectic origin for most of the cordierite is suggested by means of a reaction of the type: Bt + Sill = Crd + melt ± Kfs (R4) Cordierite and garnet (domain-II of the intermediate zone) formed through the peritectic reaction: Bt + Sil = Grt + Crd + melt ± Kfs (R5).

7.2. Thermobarometry

P-T conditions in metamorphic and igneous rocks from the intermediate and external zones were estimated by means of conventional thermobarometry (Table 3). Sample FAM143 is a Grt-Crd-Bt-Sil-Kfs bearing diatexite block from domain-II of the intermediate zone. P-T conditions for this sample were calculated with THERMOCALC v.3.33 (Powell & Holland, 1988) using the P-T average mode and the updated version of the ds55 thermodynamic dataset (November, 2003; Holland & Powell, 1998). Activity of end members for Grt, Crd, Pl, Bt, Kfs was computed with the AX software. Selected mineral compositions of garnet, cordierite and plagioclase-cores and biotite-matrix yielded T = 751 ± 51 °C and P = 4.6 ± 0.7 kbar (cor = 0.833, sigfit = 0.61). In the external zone a temperature of 700 ± 40 °C was obtained from an amphibolite (sample VCA7009, Al^{tot} in hornblende = 2.18 ± 0.19 a.p.f.u., n=7) using the Holland and Blundy (1994) Hbl-Pl geothermometer. Estimation of P-T conditions for the emplacement of the Cerro Toro complex was made on hornblende-bearing tonalites. The Holland and Blundy (1994) Hbl-Pl geothermometer and the Al-in hornblende geobarometer (Johnson and Rutherford, 1989) yielded values of T = 746 ± 40 °C and P = 5.3 ± 0.5 kbar for the external zone (ASP-120, Al^{tot} in hornblende = 2.06 a.p.f.u.). The chemical composition of hornblende (Al^{tot} = 2.10 a.p.f.u.) from tonalite of the intermediate zone (Saavedra et al. 1996) yielded similar values of 5.4 kbar (see Table 3).

In summary, temperature in the aureole ranged from ca. 700ºC in the external zone up to ca. 800ºC in the inner part of the intermediate zone. Pressure was ca. 5 kbar throughout the aureole. These results agree well with location of equilibrium reactions R2 through R5 above (§ 7.1) in P-T projection (Spear et al., 1999).

8. Whole-rock geochemistry

8.1. Major and minor elements

8.1.1.Metasedimentary rocks

Representative whole-rock analyses of migmatites (metatexites and diatexites) are given in Table 2. All the samples show a restricted range of Mg# [Mg# = 100*MgO/(MgO+FeO*) molar] between 39 and 46. Other contents are: K_2O < 3.12 wt %, Al_2O_3 ca. 13 wt % and CaO up to 1.6 wt %. The aluminum saturation index (ASI) ranges from 1.3 to 1.8. Within the migmatite group, a representative metatexite from the external zone (FAM349; SiO_2 = 59 %) and diatexites of the intermediate zone (FAM135, 143, 145, 335b and 339) are similar: SiO_2 = 60–66 %; K_2O = 3.1–4.9 wt %; FeO* = 6.2–9.0 wt %; Na_2O =

1.5–2.2 wt%; TiO_2 < 1.2 wt% and CaO ≤ 1 % (Fig. 7). ASI values range between 1.7 and 2.2. The gneisses of the external and intermediate zone (VCA1004, FAM391 and 203) have SiO_2 contents of 71–75 wt %, and are dealt with here for comparison only. In terms of trace elements, Rb content in migmatites is higher than in the gneisses, whereas Sr content is lower (Fig. 7). REE patterns of the gneisses show La_N/Yb_N ratios between 5 to 7 and weak to moderate negative Eu anomalies (Eu_N/Eu^*_N between 0.5 to 0.8) (Fig. 8a). Migmatites show LREE patterns similar to those of the gneisses; HREE however are more variable (Fig. 8a). The migmatites containing garnet (domain-II, intermediate zone) show consistently flatter patterns (La_N/Yb_N = 5.6–7.3) suggesting than HREE were retained in the garnet. Metatexites from the external zone and domain-I diatexites with cordierite and no garnet have steeper patterns (La_N/Yb_N = 9.3–17.2).

8.1.2. Tonalitic unit

The tonalitic unit (samples VCA7038, 7039, 7040, ASP115, 120, FAM213 and 175) does not show major variation in major elements (Fig. 7) with restricted contents of SiO_2 (between 60 and 63 wt %), Mg# (40–44), CaO (3.8–5.5 wt %) and alkalis (4.2–6.1 wt %). Most tonalites plot in the medium-K field on a K_2O *vs* SiO_2 diagram (Fig. 7). ASI values range from 0.97 to 1.15, i.e., metaluminous to slightly peraluminous. In contrast with major elements, Rb (10–243 ppm), Ba (41–410 ppm) and Sr (54–218 ppm) show significant scatter. The tonalitic unit shows a relative wide range of REE patterns as shown by the variable La_N/Yb_N ratio from 1.9 to 15.7 (Fig. 8b). Bt-tonalite patterns (VCA7038, 7040) do not show a Eu anomaly (Eu_N/Eu^*_N = 0.80–0.97), while the Hbl-tonalite patterns do (Eu_N/Eu^*_N = 0.40–0.82).

8.1.3. Hybrid rocks

The hybrid rocks (FAM212, 332 and 7086, Fig. 1b) show some complexities. They have restricted SiO_2 contents between 62 and 69 wt%, yield values of Mg# between 36 and 40, and are slightly peraluminous (ASI = 1.01–1.17). Like other rock types they show a decrease of FeO* with increasing SiO_2 content (Fig. 7c) but no clear trends are displayed on other Harker plots. Some components roughly follow the tonalitic unit trend (e.g., CaO or ASI *vs.* SiO_2, Fig. 7), whereas concentrations of other elements are anomalous (e.g., Na_2O or Ba) or can even be compared to those of the migmatites (i.e., K_2O and Rb *vs.* SiO_2). In the K_2O vs. SiO_2 classification diagram, the hybrid rocks fall close to the boundary between medium- and high-K fields. Chondrite-normalized REE patterns exhibit highly variable La_N/Yb_N ratios from 1.9 to 12.2 and Eu_N/Eu^*_N from 0.36 to 1.16 (Fig. 8c). Total REE content varies widely from 48 to 419 ppm.

8.1.4. Leucogranitoids

Regardless of location, leucogranitoids of the intermediate zone show a restricted range of SiO_2 between 71 and 77 wt % and a clear trend of decreasing FeO* with increasing SiO_2 (Fig. 7). However the K_2O content allows distinction of two groups that correlate with the petrographic distinction: (i) the leucogranites (FAM333, 346, 388, 394 and 397), with K_2O between 4.11 and 5.36 wt % that show a wide range of Mg# values (from 9 to 39), and (ii) the leucotonalites (FAM326, 329, 398 and 399) with K_2O between 1.02 and 1.76 wt % and Mg# values between 28 and 47. Leucotonalites show contents of Na_2O (2.9–5.08 wt %) and CaO (1.14–3.88 wt %) higher than in leucogranites (Na_2O = 2.67–3.36 wt % and CaO = 0.84–2.64 wt %), reflecting quite dissimilar modal proportions of feldspar (see Table 1 and Supplementary data). Moreover, the latter have higher contents of Rb (90–222 ppm) and very variable contents of Ba (30–694 ppm) and Sr (15–195 ppm) compared with leucotonalites: Rb (40–69 ppm), Ba (97–267 ppm) and Sr (112–171 ppm). The average ASI value of leucogranitoids is 1.04 ± 0.02. In REE patterns the leucogranites reveal a wide range of La_N/Yb_N ratios from 0.8 to 9.3 and Eu_N/Eu^*_N from 0.36 to 3.76 (Fig. 8d), whereas the leucotonalites show relatively high LREE but low to intermediate HREE values (La_N/Yb_N = 8.5–27) and mostly positive Eu anomalies (Eu_N/Eu^*_N = 1.75–3.95) (Fig. 8e).

8.2 Isotope (Sr and Nd) geochemistry

A reference age of 481 Ma for calculation of isotope compositions at the time of metamorphism/magmatism was taken from the weighted U-Pb SHRIMP zircon age of sample FAM7086, a hybrid rock from the intermediate zone (see Fig. 1b) formerly classified as an I-type tonalite by Dahlquist et al. (2008). Migmatites have $^{87}Sr/^{86}Sr_{(t)}$ values between 0.7128 to 0.7190 and εNd_t values from -6.4 to -8.3 (Table 4) Compared with the published data of three Cerro Toro tonalites ($0.7058 \leq {}^{87}Sr/^{86}Sr_{(t)} \leq 0.7096$ and $-4.9 \leq \varepsilon Ndt \leq -5.8$, Dahlquist and Galindo, 2004) the new Hbl-tonalite sample from the tonalite pluton of the internal zone (collected about 20 km to the east of the contact) yields a similar $^{87}Sr/^{86}Sr_{(t)}$ value (0.7076) but a higher εNdt (≈ -3.9). Hybrid rocks (FAM332 and FAM7086) yield $^{87}Sr/^{86}Sr_{(t)}$ values of 0.7121 and 0.7085, and εNdt values of -5.9 and -6.3 respectively that plot between those of tonalites and migmatites, apparently on an hypothetical two-component mixing line between sample FAM175 (an uncontaminated tonalite; Supplementary data) and the average isotopic composition of the metasedimentary rocks (Fig. 9). A simple calculation with a mixing-equation (Faure, 1986; eq. 9.1, page 141 and Supplementary data) suggests that hybrid rocks could be a mixture of 63% metasedimentary rocks (and/or derived melts) and 37% tonalite magma. Leucogranitoids of the intermediate domain are isotopically heterogeneous; they have $^{87}Sr/^{86}Sr_{(t)}$ ratios between 0.7061 and 0.7113, except for sample FAM394 (0.7419), and yield two groups of εNdt values (Fig. 9): most samples (group I; FAM 388, 394, 397, 398, 399; Table 4) yield values between -3.9 to -4.6. Group II (FAM 333 and 346; Table 4) with more negative values, -6.2 and -8.6.

9. DISCUSSION

9.1. Metamorphic evolution of the Cerro Toro aureole

The occurrence of peritectic cordierite and garnet in diatexites of the intermediate zone further suggests that biotite dehydration melting took place. Evidence for anatexis is provided by textures such as feldspars and cordierite showing crystal faces against quartz, simple twinning in K-feldspar, and alignment of euhedral cordierite crystals (e.g., Vernon, 2011). Moreover, some cordierite crystals grew across the foliation, implying that peak-T conditions in the intermediate zone were attained relatively late. Thus, recorded transformations started with the cordierite and garnet-absent assemblage of the external zone at a temperature of ca. 700 °C, followed inwards by domain-I assemblages with cordierite, and these in turn by higher-grade domain-II migmatites with quartz + plagioclase + biotite-2 + cordierite + garnet + K-feldspar + sillimanite at T values of ca. 750 ºC (Fig. 10). The geological and petrological evidence above suggests that at Cerro Toro, heat from the tonalite sheeted bodies affected host metamorphic rocks that before intrusion were at temperatures ≤ 700ºC. Advective heating from the tonalite was responsible for development of a metamorphic aureole with narrow mineral zones parallel to the igneous contact.

9.2. The role of the water in the partial melting of the Cerro Toro aureole

The abundance of anatectic rocks in the intermediate zone (see Fig. 1b) cannot be attributed entirely to biotite-dehydration melting in the temperature range 700-800 °C (e.g., Clemens and Vielzeuf, 1987; Patiño Douce and Johnston, 1991). This is inferred from the presence of amphibole in the hybrids containing rounded inclusions of plagioclase, quartz and metamorphic biotite-2 (Fig. 5c). This evidence suggests that water-saturated conditions were attained within the aureole to permit reactions such as Pl +

Qtz + Bt + H_2O = Hbl + L (ca. 710 °C at 5 kbar, R6 in Figure 10). In fact, partial melting experiments on quartz + plagioclase + biotite rocks show that 3-5 wt/% H_2O is required to stabilize amphibole (Naney, 1983; Conrad et al., 1988; Gardien et al., 2000). Moreover, water-fluxed melting consumes more plagioclase than micas since increasing H_2O-activity depresses the Pl + Qtz solidus (e.g., Conrad et al., 1988; Patiño Douce and Harris 1998). Thus, depletion of CaO and Sr in migmatites of the intermediate zone (see § 8.1.1) could be due to the removal of plagioclase via fluid-enhanced partial melting. On the other hand, amphibole-free hybrid/leucogranitoid rocks in this zone that contain biotite-2 with rounded outlines along with K-feldspar and titanite (see Table 1 and Fig. 5h) indicate hydration melting reactions such as: Pl + Qtz + Bt + H_2O = K-rich melt + titanite (e.g., Sawyer, 2010) or Pl + Qtz + Bt + Kfs + H_2O = L (ca. 720 °C at 5 kbar, R7 in Figure 10). We infer that the intermediate zone migmatites underwent initial metamorphism through mica-dehydration reactions that evolved into wet conditions (water fluxing) near the main tonalite pluton, producing an enhanced zone of extensive melting (Fig. 10). The cause of the inferred water-excess is unknown. However it is at least possible that fluids released deeper in the aureole by means of devolatilization reactions R1 to R4 (Figure 10) moved up-the-thermal-gradient and concentrated in the intermediate zone (e.g. Yardley and Long, 1981; Nabelek et al., 2012).

9.3. Estimate of the melt volume in diatexites

According to residue-protolith mass-balance calculations (Sawyer, 1991), if concentrations in the source (C_o), leucosome (C_L) and residue (C_r) are known, an estimate of the degree of partial melting to produce a leucosome can be estimated from the formula $C_o = FC_L + (1 - F)C_r$. However, given the difficulty of recognizing true leucosomes within the aureole, because of the mixing processes described above, an alternative approach is to rely on the source-rock and those elements that are concentrated in the residue (such as FeO*, MgO, Nb, Sc, Zn, Zr, Co and Cr), when the equation is reduced to $F = (C_r – C_o)/C_r$. The composition of the biotite-rich Grt-Crd diatexite (sample FAM143) was assumed to represent the residue, whereas an average composition of the gneiss samples (FAM391 and VCA1004) was taken as the protolith, based on the recognition of cores with gneissic texture in some migmatitic blocks (see above). The results are shown in Table 5 where it can be seen that the estimated degree of partial melting in the intermediate zone of the aureole is around 40 %. This value seems high, but experimental work with added water (~ 4 wt %, required to stabilise amphibole) and temperature about 750 °C yields values similar to this (e.g., Finger and Clemens, 1995; Patiño Douce and Harris, 1998).

9.4. Hybridization and the formation of leucogranitoids

One important issue in the Cerro Toro aureole is the evidence of hybridization in the intermediate zone, resulting from interaction between partially molten migmatite and tonalite magma. Hybrids consist of recognizable metamorphic minerals (e.g., biotite-2) and others, such as skeletal plagioclase, that could be formed (or requilibrated) after mixing (e.g., Castro, 2001; Erdmann et al., 2007). This plagioclase has a composition intermediate between those of the tonalite and migmatite and experienced temperatures (~ 750 °C), well above the wet solidus (ca. 690 °C at 6 kbar, Watkins et al., 2007). Moreover, a transition is recognized from these hybrids to leucogranitoids involving progressive loss of metamorphic foliation at the outcrop scale. In fact, the biotite-2 content (ca 10 %) in domain-III hybrids is much lower than in domain-II hybrids (ca. 20%) suggesting that the former involved a higher degree of melting, by means of reactions R6 and R7 above. In turn Bt-poor hybrids gradually pass into massive leucogranitoids; the latter representing a melt-crystal mixture without relics of a metamorphic fabric. Partially resorbed plagioclase cores in leucogranitoids with dissimilar compositions (An_{37-43} and An_{18-21}; Fig. 11) but with An_{26-36} overgrowths imply that the leucogranitoid magma evolved after the hybrid magma, and that $An_{\sim 30}$ crystallized on inherited plagioclase nuclei (antecrysts).

Leucogranitoid magma differentiated in turn, probably because of magma-mobility enhanced by tectonic deformation within the aureole. Leucotonalites (e.g., FAM 326, 398, 399) containing anhedral to subhedral plagioclase (with a wide range of compositions: An_{17-42}) ± biotite-2, together with high contents of Ca, Na and Sr and REE-patterns with Eu-positive anomalies, can be interpreted as a crystalline residuum after the former leucogranitoid magma. Leucogranites (e.g., FAM 397) consisting of euhedral plagioclase (An_{11-25}), microcline and biotite-3, with a genuine granitic texture, formed in turn from the residuum-free K-rich magma. They in fact have high contents of K, Rb and REE-patterns and most show Eu-negative anomalies compatible with this interpretation. Some granitic rocks (e.g., FAM 333, 399) with intermediate petrographic characteristics, i.e., equal crystal and melt-rich parts, and with intermediate contents of Ca, Na, K, Rb and Sr, and REE-patterns with a Eu-positive anomaly (see above), probably formed with retention of K-rich melt within the crystalline residuum. Thus, separation of melt from crystals after hybridization may explain the variety of textural and geochemical features shown by leucogranitoids in the intermediate zone of the aureole.

9.4.1. Geochemical constraints: Major and trace element composition

The K_2O *vs* FeO^t+MgO plot (Fig. 12a) helps to distinguish residual ferromagnesian phases from anatectic melt (e.g., Milord et al., 2001), and clearly shows that the migmatites and gneisses can be described by a combination of quartz + plagioclase and biotite vectors. The contribution of the quartz + plagioclase vector is more marked in gneisses, whereas the biotite vector predominates in migmatites, consistent with the presence of restitic minerals in the latter. Despite the presence of peritectic phases (cordierite or garnet) in the migmatite blocks of the intermediate zone, the latter do not show a trend towards cordierite in Fig. 12a. As for the leucogranitoids, the leucogranites plot along the fractionated melt vector following a clear trend of K_2O-enrichment while the leucotonalites fall near the Qtz + Pl vector (Fig. 12a). These compositional trends may be due to fractional crystallization (e.g., Sawyer 1987; Milord et al., 2001) yielding a (quartz + plagioclase)-dominated cumulate and a K-feldspar rich fractionated melt. However, the petrographic data above suggest that the leucotonalites do not correspond to pure magmatic cumulate but to a mixture of residue (dominant) and cumulates. On the K_2O *vs* CaO+Na_2O diagram (Fig. 12b, incompatible versus compatible elements) leucogranites and leucotonalites define separate fields consistent with melt-rich and residuum-rich rocks derived from anatexis (e.g., Sawyer, 2010). However, both fields are shifted towards higher CaO+Na_2O values compared to the field of the supposed migmatite protolith, i.e., the gneiss. Both are closer to the fields of the hybrids and the tonalites. As in the case of these elements contained in plagioclase, the hybrids show enrichment in Sr but not in Rb when compared with the diatexite rocks (Fig. 7). The diatexites show enrichment in K_2O and lower CaO + Na_2O contents compared to the gneisses, as expected from the increased amount of residual biotite and some K-feldspar after extraction of the anatectic melt.

9.4.2. Leucogranitoids and comparisons with experimental melt compositions

Experimental melt compositions obtained from fertile metasedimentary rock types (e.g., greywacke or pelite) are peraluminous and felsic (Montel and Vielzeuf, 1997; Patiño Douce, 1999). These mostly plot in the field of leucogranite in the A-B diagram (figure 12c), often showing a vertical trend similar to those from High Himalayas (e.g., Debon and Le Fort, 1983). When compared with these experimental melt compositions, our leucogranitoids plot partly in the same field (leucogranite) but outside the experimental melt compositions and without a visible vertical trend. They have very low values of A (= Al-Na-K-2Ca ≤ 15, i.e. a deficit in alumina), indicating a dominant quartzo-feldspathic component. This allows us to hypothesize that our leucogranitoids do not represent pure anatectic crustal melts but involve other components, such as restite minerals and/or mixing with metaluminous-derived liquids (Montel and Vielzeuf, 1997; Patiño Douce, 1999).

9.4.3 Sr - Nd isotope evidence

Major minerals of end-member magmas, i.e, tonalite and anatectic magma, involved in hybridization probably retain their isotopic composition in the hybrid magma (Beard, 2008). In the case of the Cerro Toro aureole, plagioclase controlled the distribution of Sr between the solid and liquid fractions. As explained above, the leucogranitoids contain textural evidence of inherited pre-existing plagioclase crystals (antecrysts), often partially dissolved, suggesting that they formed earlier by crystal–melt separation from hybrid magmas (e.g., Beard, 2008). This explains why the $^{87}Sr/^{86}Sr$ values are lower than those of migmatites (see § 8.2). Figure 13 shows a conceptual model for the formation of leucogranitoids. The plot of $^{87}Sr/^{86}Sr$ against Sr (Fig. 14) shows that the leucogranitoids are isotopically intermediate between the migmatites and tonalites. Samples with visible partially dissolved antecrysts (Figs. 5e, g and i) have lower $^{87}Sr/^{86}Sr$ values than antecryst-poor samples (e.g., FAM397 - Fig. 5f).

Additionally, solubility of monazite in felsic melts only occurs between 800 and 1400 °C (Montel, 1993). In consequence monazite in the Cerro Toro aureole (T between 700 and 800°C) was mostly retained in the residual assemblage of migmatites, thus leading to Nd-isotope disequilibrium melting (Watson and Harrison, 1984). In fact, εNd values of hybrids and leucogranitoids (group I) less negative than migmatites imply that monazite was not a significant contributor to the Nd budget of these magmas. However group II leucogranitoids with εNd values between -6.2 and -8.6 largely retained the Nd isotope composition of the migmatite, i.e., dominated by monazite, whilst having the $^{87}Sr/^{86}Sr$ composition of tonalites and the petrographic and chemical composition of a leucogranite. These leucogranitoids probably equilibrated with the residual mineralogy (retained or near the source) or incorporated some metamorphic monazite during further injection along the contact with migmatites in the tectonic-enhanced dynamic setting of the aureole. In fact, both samples of this group were collected from leucogranitoids surrounding migmatite blocks. This implies that the magmas either segregated fast and/or that accessories included mostly in biotite-2 were shielded during water-fluxed melting (e.g., Rubie and Brearley, 1990; Carrington and Watt, 1995; Nabelek and Glascock, 1995; Jung et al., 1999; Zeng et al., 2005).

10. Conclusions

The evidence presented here suggests that the Cerro Toro aureole is a remarkable example of pluton–wall-rock interaction coeval with regional metamorphism and deformation at mid-crustal levels. The main processes involved in the aureole were:

(1) Sheeted tonalite intrusions were emplaced at the start of the Famatinian orogeny (ca. 480 Ma) into already hot (ca 700 °C) metamorphic rocks that were separated into screens or disrupted blocks by the tonalite magma. The host rocks were metatexites.

(2) Increasing temperature within the aureole up to ca. 800ºC at the contact with the main tonalite intrusion triggered mica-dehydration melting reactions in the migmatites, that produced peritectic cordierite followed by cordierite-garnet.

(3) An increase in water activity probably took place due to hypothetical up-gradient flow of water from deeper in the aureole. The change from “dry” to “wet” conditions triggered the complementary melting of plagioclase + quartz, increasing the amount of anatectic melt in the migmatites up to 40%, and promoting the loss of continuity of the solid mineral framework.

(3) Hybrid magmas developed by mingling/mixing of tonalite with anatectic magmas in the zone closer to the main tonalite pluton (internal zone). Hybrid rocks show petrographic and geochemical characteristics intermediate between these end-members.

(4) Variable separation of melt and crystals after hybridization gave rise to leucogranitoid magmas (leucotonalites and leucogranites) that were isotopically heterogeneous, with $^{87}Sr/^{86}Sr$ ratios lower and εNd values less negative, respectively, than the migmatites. However, minor leucogranitoids equilibrated with the residual mineralogy or incorporated restitic monazite, resulting in more negative εNd values.

Our results suggest that assimilation of country rocks (affected by pre- or syn-regional metamorphism) through partial melting during the emplacement of thick tonalitic magma bodies in the middle crust was an important mechanism in the case of the Cerro Toro aureole. Emplacement in the middle crust favoured longer magma-residence time that resulted in effective contamination by assimilation as compared to epizonal intrusions. This supports the idea that the chemistry of Cordilleran magmas does not only reflect their ultimate source characteristics in the subcontinental mantle: they can also undergo prolonged open system magmatic evolution in the middle crust. Under these circumstances, whole-rock isotopic ratios and model ages derived from them must be interpreted with caution.

Acknowledgements

Funds were provided by Spanish MICINN grant CGL2009-07984/BTE and an Argentinean PICT 1009 grant. We are grateful to S.R. Paterson (USC) for critical review of an earlier draft of this manuscript. P.H. Alasino thanks Carlos Bustamante and Sergio de La Vega for technical support. We thank C.G. Barnes (TTU), J.E. Otamendi (UNRC) and S. Erdmann (UO) for their very constructive reviews that significantly improved the manuscript. We also would like to thank N. Eby (editor) for your comments and suggestions to our manuscript.

References

Barnes, C.G., Yoshinobu, A.S., Prestvik, T., Nordgulen, Ø., Karlsson, H.R., Sundvoll, B., 2002. Mafic Magma Intraplating: Anatexis and Hybridization in Arc Crust, Bindal Batholith, Norway. Journal of Petrology 43, 2171-2190.

Beard, J.S., Ragland, P.C., Crawford, M.L., 2005. Reactive bulk assimilation: A model for crust-mantle mixing in silicic magmas. Geology 33, 681-684.

Beard, J.S., 2008. Crystal-Melt separation and the development of isotopic heterogeneities in hybrid magmas. Journal of Petrology 49, 1027-1041.

Büsch, W., Schneider, G., Mehnert, K.R., 1974. Initial melting at grain boundaries part II: melting of rocks of granodioritic, quartzdioritic and tonalitic composition. Neues Jahrbuch für Mineralogie Abhandlungen 1974, 345–370.

Carrington, D.P., Watt, G.R., 1995. A geochemical and experimental study of the role of K-feldspar during water-undersaturated melting of metapelites. Chemical Geology 122, 59-76.

Casquet, C., Rapela, C.W., Pankhurst, R.J., Baldo, E.G., Galindo, C., Fanning, C.M., Dahlquist, J.A., 2012. Fast sediment underplating and essentially coeval juvenile magmatism in the Ordovician margin of Gondwana, Western Sierras Pampeanas, Argentina. Gondwana Research 22, 664–673.

Castro, A., 2001. Plagioclase morphologies in assimilation experiments. Implications for disequilibrium melting in the generation of granodiorite rocks. Mineralogy and Petrology 71, 31-49.

Castro, A., Martino R., Vujovich, G., Otamendi, J., Pinotti, L., d'Eramo, F., Tibaldi, A., Viñao, A. 2008. Top-down structures of mafic enclaves within Valle Fértil magmatic complex (Early Ordovician, San Juan, Argentina). Geologica Acta 6, 217-229.

Castro, A., Díaz-Alvarado, J., Fernández, C., 2013. Fractionation and incipient self-granulitization during deep-crust emplacement of Lower Ordovician Valle Fértil batholith at the Gondwana active margin of South America. Gondwana Research, http://dx.doi.org/10.1016/j.gr.2012.08.011

Cawood, P.A., 2005. Terra Australis Orogen: Rodinia breakup and development of the Pacific and Iapetus margins of Gondwana during the Neoproterozoic and Paleozoic. Earth-Science Reviews 69, 249–279.

Clarke, D.B., 2007. Assimilation of xenocrysts in granitic magmas: principles, processes, proxies, and problems. Canadian Mineralogist, 45, 5-30.

Clemens, J.D., Vielzeuf, D., 1987. Constraints on melting and magma production in the crust. Earth and Planetary Science Letters 86, 287-306.

Conrad, W.K., Nicholls, I.A., Wall, V.J., 1988. Metaluminous and peraluminous crustal compositions at 10 kb: evidence for the origin of silicic magmas in the Taupo Volcanic Zone, New Zealand, and other occurrences. Journal of Petrology 29, 765–803.

Cristofolini, E.A., Otamendi, J.E., Ducea, M.N., Pearson, D.M., Tibaldi, A.M., Baliani, I., 2012. Detrital zircon U–Pb ages of metasedimentary rocks from Sierra de Valle Fértil: entrapment of Middle and Late Cambrian marine successions in the deep roots of the Early Ordovician Famatinian arc. Journal of South American Earth Sciences 37, 77–94.

Dahlquist, J.A., Galindo, C., 2004. Geoquímica isotópica de los granitoides de la sierra de Chepes: un modelo geotectónico y termal, implicancias para el orógeno famatiniano. Revista de la Asociación Geológica Argentina, 59, 57-69.

Dahlquist, J.A., Alasino, P.H., 2005. Hallazgo de Granitoides fuertemente peraluminosos en la Sierra de Famatina: implicancias petrogenéticas para el Orógeno Famatiniano. Revista de la Asociación Geológica Argentina 60: 301-310.

Dahlquist, J.A., Rapela, C.W., Baldo, E.G., 2005. Cordierite-bearing S-type granitoids in the Sierra de Chepes (Sierras Pampeanas): petrogenetic implications. Journal of South American Earth Science 20, 231-251.

Dahlquist, J.A., Galindo, C., Pankhurst, R.J., Rapela, C.W., Alasino, P.H., Saavedra, J., Fanning, C.M., 2007. Magmatic evolution of the Peñón Rosado granite: petrogenesis of garnet- bearing granitoids. Lithos, 95, 177-207.

Dahlquist, J.A., Pankhurst, R.J., Rapela, C.W., Galindo, C., Alasino, P., Fanning, C.M., Saavedra, J., Baldo, E., 2008. New SHRIMP U–Pb data from the Famatina complex: constraining Early–Mid Ordovician Famatinian magmatism in the Sierras Pampeanas, Argentina. Geologica Acta 6, 319-333.

Dahlquist, J.A., Pankhurst, R.J., Gaschnig, R.M., Rapela, C.W., Casquet, C., Alasino, P.H., Galindo, C., Baldo, E.G., 2013. Hf and Nd isotopes in Early Ordovician to Early Carboniferous granites as monitors of crustal growth in the Proto-Andean margin of Gondwana. Gondwana Research, http:c//dx.doi.org/10.1016/j.gr.2012.08.013.

Debon, F., Le Fort, P., 1983. A chemical–mineralogical classification of common plutonic rocks and associations. Transactions of the Royal Society of Edinburgh, Earth Sciences 73, 135–149.

De Paolo, D.J., Linn, A.M., Schubert, G., 1991. The continental crustal age distribution: methods of determining mantle separation ages from Sm-Nd isotopic data and application to the Southwestern United States. Journal of Geophysical Research 96, 2071-2088.

Ducea, M.N., Otamendi, J.E., Bergantz, G., Stair, K.M., Valencia, V.A., Gehrels, G.E., 2010. Timing constraints on building an intermediate plutonic arc crustal section: U–Pb zircon geochronology of the Sierra de Valle Fértil-La Huerta, Famatinian arc, Argentina. Tectonics 29, TC 4002. http://dx.doi.org/10.1029/2009TC002615.

Erdmann, S., London, D., Morgan VI, G.B., Clarke, D.B., 2007. The contamination of granitic magma by metasedimentary country-rock material: an experimental study. The Canadian Mineralogist 45, 43-61.

Erdmann, S., Jamieson, R.A., Michael A. MacDonald, M.A., 2009. Evaluating the Origin of Garnet, Cordierite, and Biotite in Granitic Rocks: a Case Study from the South Mountain Batholith, Nova Scotia. Journal of Petrology 50, 1477-1503.

Faure, G., 1986. Principles of isotope geology, Second Edition. John Wiley & Sons.

Finger, F., Clemens, J.D., 1995. Migmatization and "secondary" granitic magmas: effects of emplacement and crystallization of "primary" granitoids in Southern Bohemia, Austria. Contributions to Mineralogy and Petrology 120, 311-326.

Gardien, V., Thompson, A.B., Ulmer, P., 2000. Melting of biotite+plagioclase+quartz gneisses: the role of H_2O in the stability of amphibole. Journal of Petrology 41, 651–666.

Greenfield, J. E., Clarke, G.L., Bland, M., Clark, D. J., 1996. *In-situ* migmatite and hybrid diatexite at Mt Stafford, central Australia. Journal of Metamorphic Geology 14**,** 413-426.

Harris, N., McMillan, A., Holness, M., Uken, R., Watkeys, M.K., Rogers, N. & Fallick A., 2003. Melt generation and fluid flow in the thermal aureole of the Bushveld Complex, Journal of Petrology 44, 1031-1054.

Holland, T.J.B., Blundy, J.D., 1994. Non-ideal interactions in calcic amphiboles and their bearing on amphibole-plagioclase thermometry. Contributions to Mineralogy and Petrology 116, 433-447.

Holland, T.J.B. and Powell, R., 1998. An internally-consistent thermodynamic dataset for phases of petrological interest. Journal of Metamorphic Geology 16, 309-344.

Holtz, F., Johannes, W., 1991. Genesis of peraluminous granites I. Experimental investigation of melt compositions at 3 and 5 kbar and various H_2O activities. Journal of Petrology 32, 935-957.

Jarosewich, E., Nelen, J.A., Norberg, J.A., 1980. Reference samples for electron microprobe analysis. Geostandards Newsletter 4, 43–47.

Johnson, M.C., Rutherford, M.J., 1989. Experimental calibration of the aluminiun-in-hornblende geobarometer with application to Long Valley Caldera (California) volcanic rocks. Geology 17, 837-41.

Johnson, D.M., Hooper, P.R., Conrey, R.M., 1999. XRF analysis of rocks and minerals for major and trace elements on a single low dilution Li-tetraborate fused bead. Advances in X-ray Analysis 41, 843–867.

Jordan, T.E. and Allrnendinger, R.W., 1986. The Sierras Pampeanas of Argentina: a modern analogue of Rocky Mountain foreland deformation. American Journal of Sciences, 286, 737-764.

Jung, S., Hoernes, S., Masberg, P, Hoffer, E., 1999. The petrogenesis of some migmatites and granites (Central Damara Orogen, Namibia): Evidence for disequilibrium melting, wall-rock contamination and crystal fractionation. Journal of Petrology, 40, 1241-1269.

Kerrick, D. M., 1970, Contact metamorphism in some areas of the Sierra Nevada,. California: Geological Society of America Bulletin 81, 2913–2938.

Kretz, R., 1983. Symbols for rock-forming minerals. American Mineralogist 68, 277–279.

Le Maitre, R. W., Bateman, P., Dudek, A., Keller, J., Lameyre, J., Le Bas, M. J., Sabine, P. A., Schmid, R., Sorensen, S., Streckeisen, A., Woolley, A.R. & Zanettin, B., 1989. A Classification of Igneous Rocks and Glossary of Terms. Oxford: Blackwell Scientific.

McGuire, A.V., Francis, C.A., Diar, M.D., 1992. Mineral standards for electron microprobe analysis of oxygen. American Mineralogist 77, 1087–1091.

Miller, H., Söllner, F., 2005. The Famatina Complex (NW Argentina): back-docking of an island arc terrane accretion? Early Palaeozoic geodynamics at the western Gondwana margin, in: Vaughan, A.P.M., Leat, P.T., Pankhurst, R.J. (Eds.), Terrane Processes at the Margins of Gondwana. Journal of the Geological Society of London, Special Publications, 246, 241-256.

Milord, I., Sawyer, E.W., Brown, M., 2001. Formation of diatexite migmatites and granite magma during anatexis of metasedimentary rocks: An example from St. Malo, France. Journal of Petrology 42, 487-505.

Montel, J.-M., 1993. A model for monazite/melt equilibrium and the application to the generation of granitic magmas. Chemical Geology 110**,** 127-146.

Montel, J.M., Vielzeuf, D., 1997. Partial Melting of metagreywackes, Part II. Compositions of minerals and melts. Contribution to Mineralogy and Petrology 128, 176-196.

Nabelek, P.I., Glascock, M.D., 1995. REE-depleted leucogranites, Black Hills, South Dakota: a consequence of disequilibrium melting of monazite-bearing schists. Journal of Petrology 36, 1055–71.

Nabelek, P.I., Hofmeister, A., Whittington, A.G., 2012. The influence of temperature-dependent thermal diffusivity on the conductive cooling rates of plutons and temperature-time paths in contact aureoles. Earth and Planetary Science Letters 317, 157–164.

Nakamura, N., 1974. Determination of REE, Ba, Mg, Na and K in carbonaceous and ordinary chondrites. Geochimica et Cosmochimica Acta 38, 757-773.

Naney, M.T., 1983. Phase equilibria of rock-forming ferromagnesian silicates in granites systems. American Journal of Science, 283, 993-1033.

Otamendi, J.E., Ducea, M.N., Tibaldi, A.M., Bergantz, G., de la Rosa, J.D., Vujovich, G.I., 2009. Generation of tonalitic and dioritic magmas by coupled partial melting of gabbroic and metasedimentary rocks within the deep crust of the Famatinian magmatic arc, Argentina. Journal of Petrology 50, 841–873.

Otamendi, J.E., Ducea, M.N., Bergantz, W., 2012. Geological, petrological and geochemical evidence for progressive construction of an arc crustal section, Sierra de Valle Fértil, Famatinian Arc, Argentina. Journal of Petrology 53, 761-800.

Pankhurst, R.J., Rapela, C.W., Saavedra, J., Baldo, E., Dahlquist, J., Pascua, I. & Fanning, C.M., 1998. The Famatinian magmatic arc in the southern Sierras Pampeanas, in Pankhurst, R.J., Rapela , C.W.

(Eds), The Proto-Andean Margin of Gondwana. Geological Society of London, Special Publications 142, 343-367.

Pankhurst, R.J., Rapela, C.W., Fanning, C.M., 2000. Age and origin of coeval TTG, I–S-type granites in the Famatinian belt of NW Argentina. Transactions of the Royal Society of Edinburgh, Earth Sciences 91, 151-168.

Paterson, S.R., Vernon, R.H., Fowler, T.K., 1991. Aureole tectonics. Mineralogical Society of America Reviews in Mineralogy 23, 673-722.

Paterson, S., Farris, D., 2008. Downward host rock transport and the formation of rim monoclines during the emplacement of Cordilleran batholiths. Transactions of the Royal Society of Edinburgh: Earth Sciences, 97, 397-413.

Patiño Douce, A.E., 1999. What do experiments tell is about the relative contributions of the crust and mantle to the origin of granitic magmas?, in: Castro, A., Fernandez, C. and Vigneresse, J., (Eds.), Understanding Granites: Integrating New and Classical Techniques. Geological Society, London, Special Publications 168, 55-75.

Patiño Douce, A.E., Johnston, A.D., 1991. Phase equilibria and melt productivity in the pelitic system: implications for the origin of peraluminous granitoids and aluminous granulites. Contribution to Mineralogy and Petrology 107, 202-218.

Patiño Douce, A.E., Harris, N., 1998. Experimental constraints on Himalayan Anatexis. Journal of Petrology, 39, 689-710.

Pattison, D.R.M., 1992. Stability of andalusite and sillimanite and the Al_2SiO_5 triple point: constraints from the Ballachulisch aureole. Scottish Journal of Geology 100, 423-446.

Pattison, D.R.M., Harte, B., 1985. A petrogenetic grid for pelites in the Ballachulish and other Scottish thermal aureoles. Journal of the Geological Society of London 142**,** 7-28.

Peterson, J.W. and Newton, R.C., 1989. Reversed experiments on biotite-quartz-feldspar melting in the system KMASH*:* implications for crustal anatexis. Journal of Geology 97: 465-486.

Powell, R., Holland, T.J.B., 1988. An internally consistent data set with uncertainties and correlations: 3. Applications to geobarometry, worked examples and a computer program. Journal of Metamorphic Geology 6, 173-204.

Rapela, C.W., Toselli, A., Heaman, L., Saavedra, J., 1990. Granite plutonism of the Sierras Pampeanas: an inner cordilleran Paleozoic arc in the Southern Andes, in: Kay, S.M., Rapela, C.W. (Eds.), Plutonism from Antarctica to Alaska: Geological Society of America, Special Paper, 241, pp. 77–90.

Rastall, R.h., 1910. The Skiddaw granite and its metamorphism. Quarterly Journal of the Geological Society of London, 66. 116-141.

Rubie, D.C., Brearley, A.J., 1990. A model for rates of disequilibrium melting during metamorphism, in: Ashworth, J.R., Brown, M. (Eds.), High Temperature Metamorphism and Crustal Anatexis. Unwin Hyman, London 57-86.

Saavedra, J., Pellitero, E., Rossi, J., Toselli, A., 1992. Magmatic evolution of the Cerro Toro granite, a complex Ordovician pluton of Northwestern Argentina. Journal of South American Earth Science, 5, 21-32.

Saavedra, J., Toselli, A., Rossi, J., Pellitero, E., 1996. Granitoides y rocas básicas del Cerro Toro, in: Aceñolaza, F.G., Miller, H., Toselli, A.J. (Eds.), Geología del Sistema de Famatina. Münchner Geologische Hefte, Reihe A, 19(6), 229-240.

Saavedra, J., Toselli, A., Rossi, J., Pellitero, E., Durand, F., 1998. The Early Palaeozoic magmatic record of the Famatina System: a review, in: Pankhurst, R.J., Rapela, C.W. (Eds.), The Proto-Andean Margin of Gondwana. Journal of the Geological Society of London, Special Publication, 142, 283-295.

Saito, S., Arima, M., Nakajima, T., 2007. Hybridization of a shallow 'I-type' granitoid pluton and its host migmatite by magma-chamber wall collapse: the Tokuwa Pluton, Central Japan. Journal of Petrology, 48, 79-111.

Sawyer, E.W., 1987. The role of partial melting and fractional crystallization in determining discordant migmatite leucosome compositions. Journal of Petrology 28, 445-473.

Sawyer, E.W., 1991. Disequilibrium Melting and the Rate of Melt–Residuum Separation During Migmatization of Mafic Rocks from the Grenville Front, Quebec. Journal of Petrology 32, 701-738.

Sawyer, E.W., 1999. Criteria for the recognition of partial melting. Physics and Chemistry of the Earth 24, 269-279.

Sawyer, E.W., 2008. Atlas of Migmatites, Canadian Mineralogist Special Publication 9, Mineralogical Association of Canada, Quebec, Canada, 373 pp.

Sawyer, E.W., 2010. Migmatites formed by water-fluxed partial melting of a leucogranodiorite protolith: Microstructures in the residual rocks and source of the fluid. Lithos 116, 273–286

Spear, F.S. and Cheney, J.T., 1989. A petrogenetic grid for pelitic schists in the system SiO_2 - Al_2O_3 - FeO - MgO - K_2O - H_2O. Contributions to Mineralogy and Petrology, 101, 149-164.

Spear, F.S., Matthew, J.K., Cheney, J.T., 1999. *P-T* paths from anatectic pelites. Contributions to Mineralogy and Petrology 134, 17-32.

Steiger, R.H., Jäger, E., 1977. Subcommision of geochronology: convention on the use of decay constants in geo- and chosmochronology. Earth Planet. Sci. Lett. 1, 369–371.

Toselli, A.J., Rossi de Toselli, J.N., Saavedra, J., Pellitero, E., Medina, M.E., 1988. Aspectos Petrológicos y Geoquímicos de los Granitoides del entorno de Villa Castelli, Sierras Pampeanas Occidentales - Sistema de Famatina. 5° Congreso Geológico Chileno, Actas 3: I1 7-I28.

Ugidos, J.M., Recio, C., 1993. Origin of cordierite-bearing granites by assimilation in the Central Iberian Massif (CIM), Spain. Chemical Geology 103, 27–43.

Vernon, R.H., 2004. A Practical Guide to Rock Microstructure. Cambridge, UK, Cambridge University Press, 594 pp.

Vernon, R.H., 2011. Microstructures of melt-bearing regional metamorphic rocks, in van Reenen, D.D., Kramers, J.D., McCourt, S., Perchuk, L.L. (Eds.), Origin and Evolution of Precambrian High-Grade Gneiss Terranes, with Special Emphasis on the Limpopo Complex of Southern Africa: Geological Society of America Memoir 207, 1–11.

Vidal, P., Cocherie, A., Le Fort P., 1982. Geochemical investigations of the origin of the Manaslu leucogranite (Hymalaya Nepal). Geochimica et Cosmochimica Acta 46, 2279-2292.

Vielzeuf, D., Holloway, J.R., 1988. Experimental determination of the fuid-absent melting relations in the pelitic system. Consequence for crustal differentiation. Contributions to Mineralogy and Petrology 98, 257-276.

Villaseca, C., Barbero, L., Herreros, V., 1998. A re-examination of the typology of peraluminous granite types in intracontinental orogenic belts. Transactions of the Royal Society of Edinburgh, Earth Sciences 89, 113–119.

Watkins, J.M., Clemens, J.D., Treloar, P.J., 2007. Archaean TTGs as sources of younger granitic magmas: melting of sodic metatonalites at 0.6–1.2 GPa. Contributions to Mineralogy and Petrology 154, 91–110.

Watson, E.B., Harrison, T.M., 1984. Accessory minerals and the geochemical evolution of crustal magmatic systems: a summary and prospectus of experimental approaches. Physics of the Earth and Planetary Interiors 35, 19–30

Yardley B.W.D., Long, C.B., 1981. Contact metamorphism and fluid movement around the Easky adamellite, Ox Mountains, Ireland. Mineralogical Magazine 44, 125-131.

Yardley B.W.D., Barber, J.P., 1991. Melting reactions in the Connemara Schists: The role of water infiltration in the formation of amphibolite facies migmatites. American Mineralogist, 76, 848-856.

Zeng, L., Saleeby, J. B., Asimow, P., 2005. Nd isotope disequilibrium during crustal anatexis: a record from the Goat Ranch migmatite complex, southern Sierra Nevada batholith, California. Geology 33, 53-56.

Figure 1. Alasino et al.

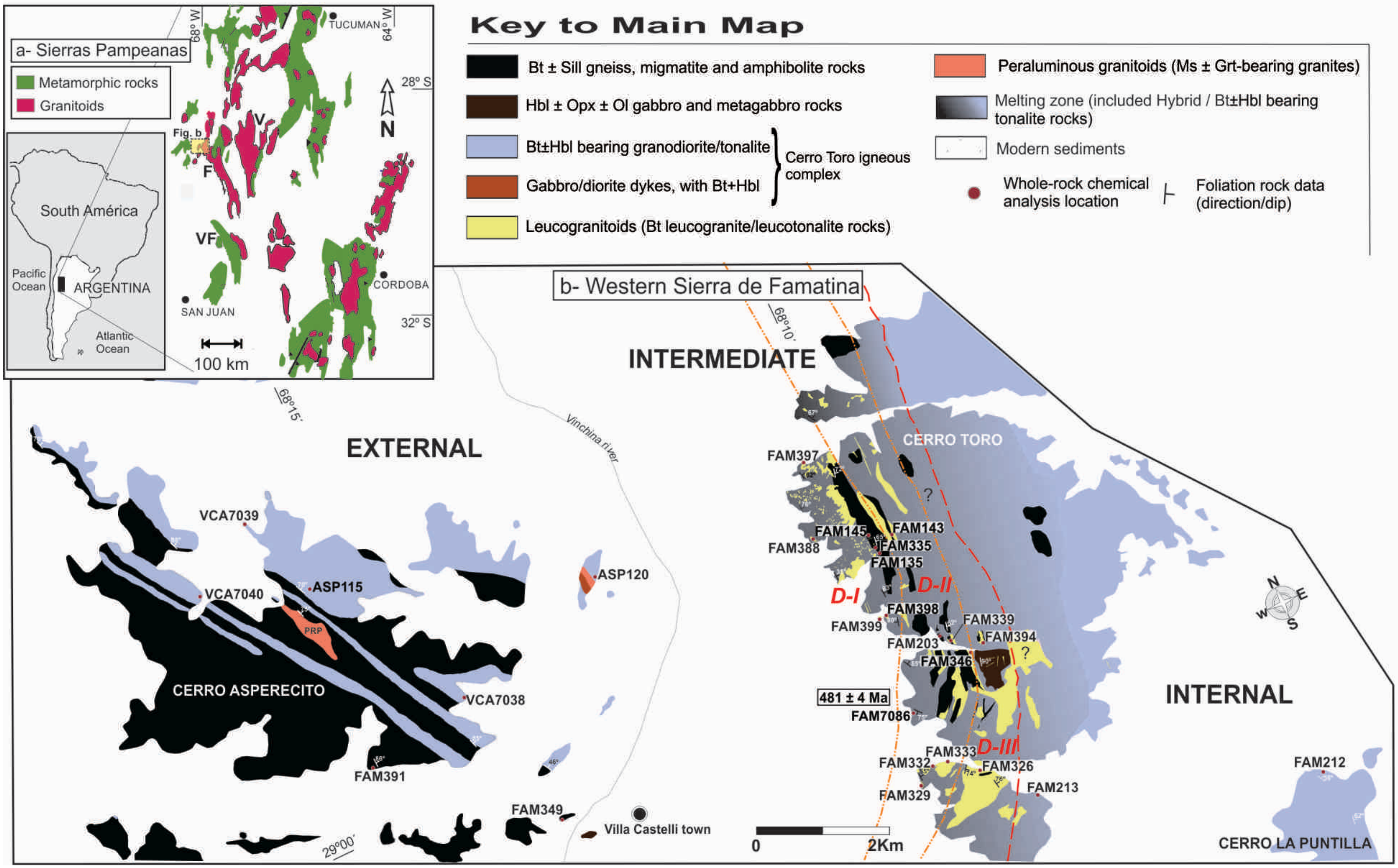

Figure 2. Alasino et al.

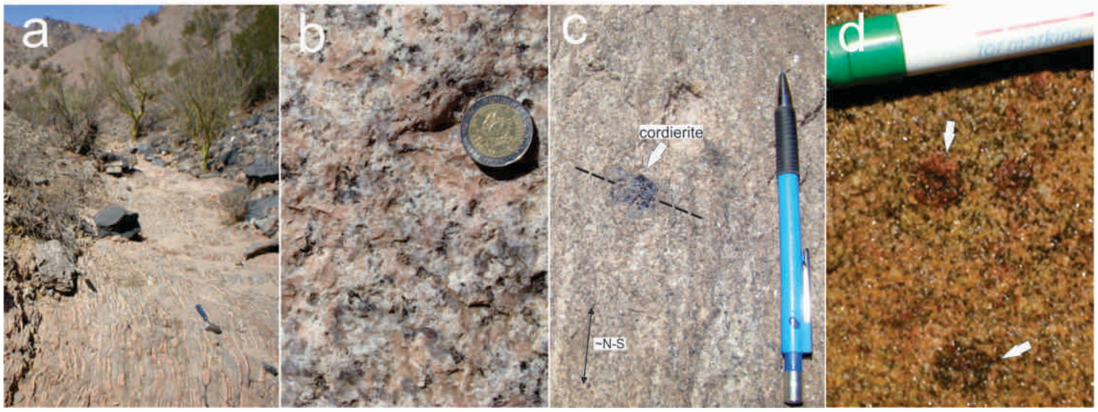

Figure 3. Alasino et al.

Figure 4. Alasino et al.

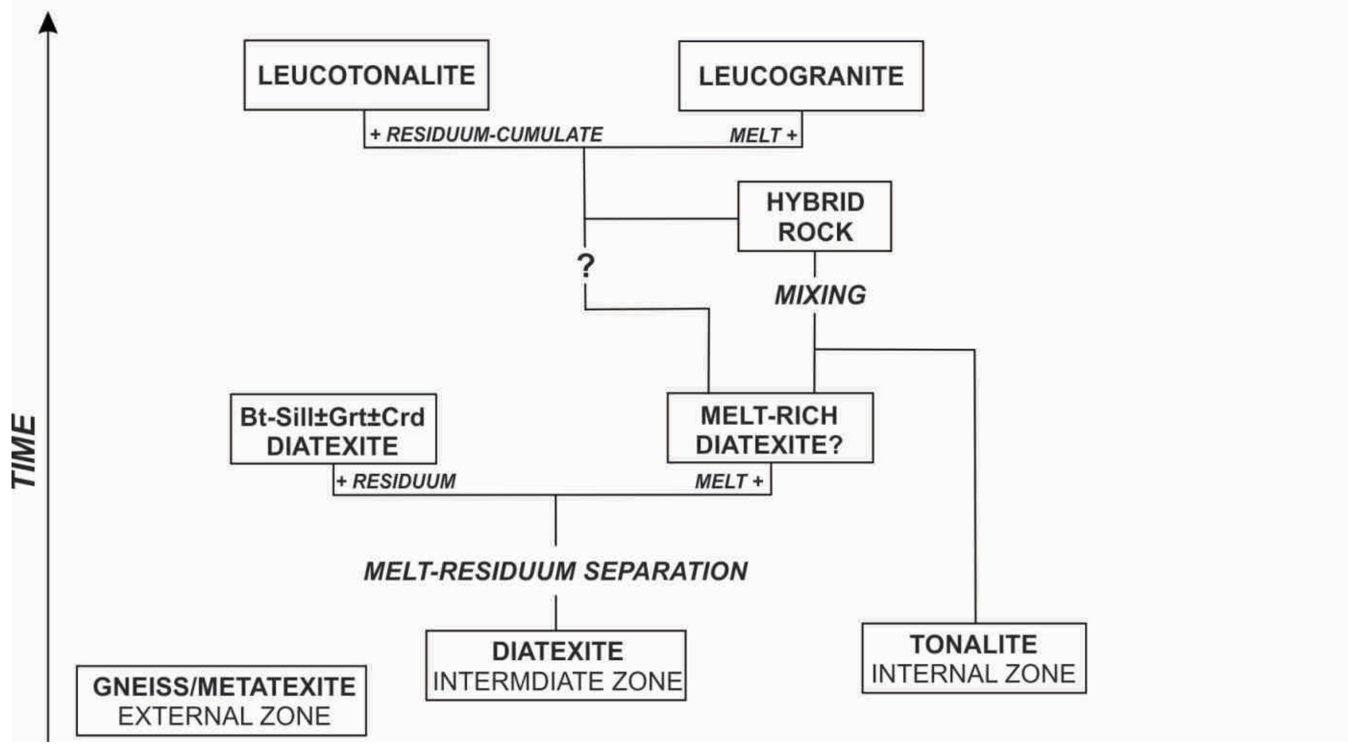

Figure 5. Alasino et al.

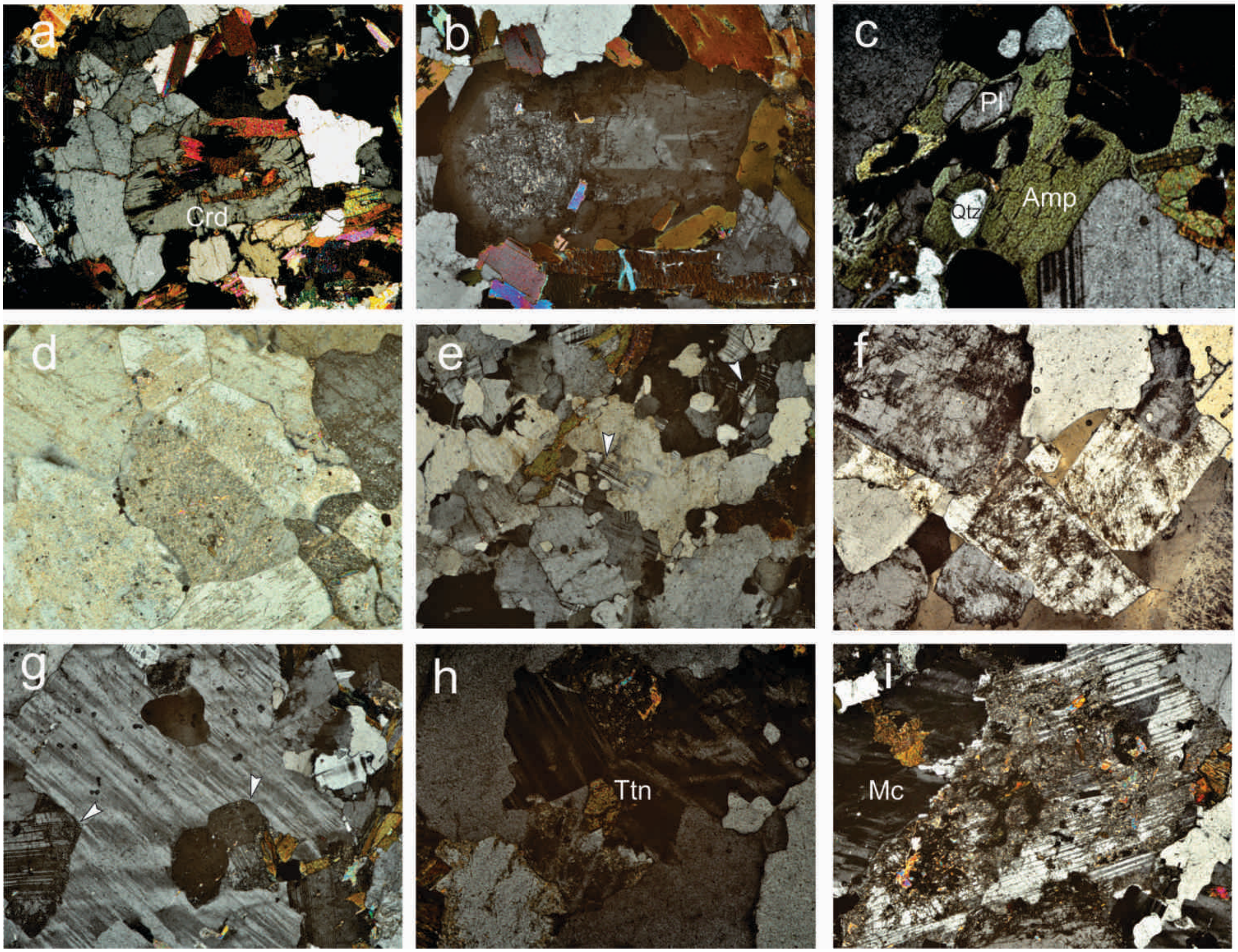

Figure 6. Alasino et al.

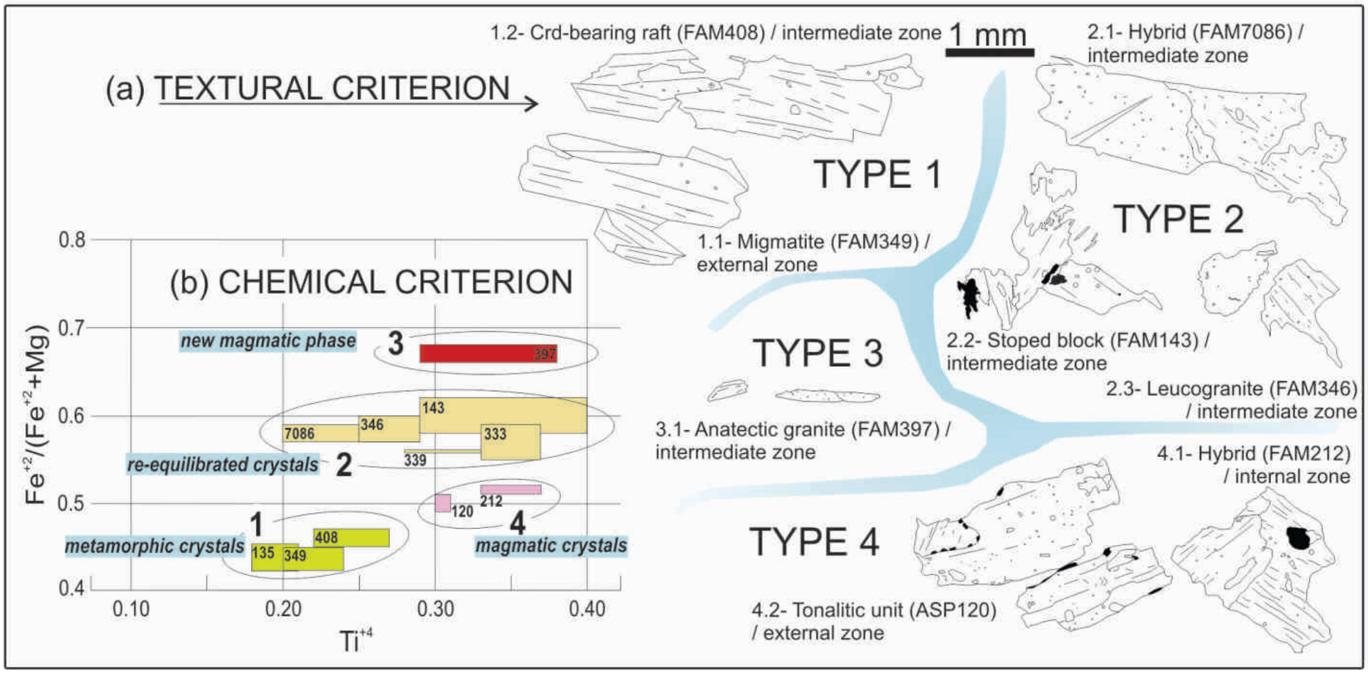

Figure 7. Alasino et al.

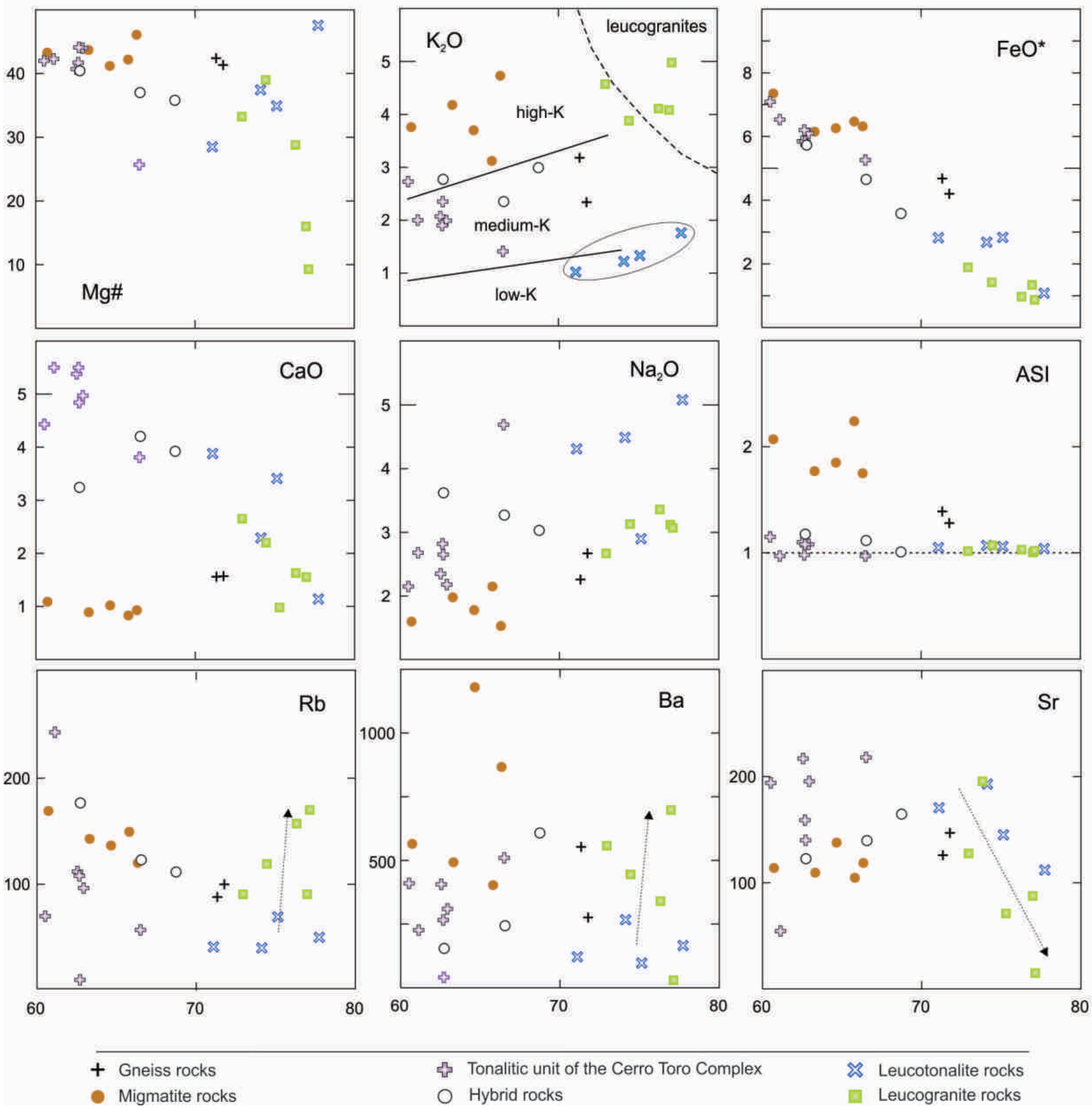

Figure 8. Alasino et al.

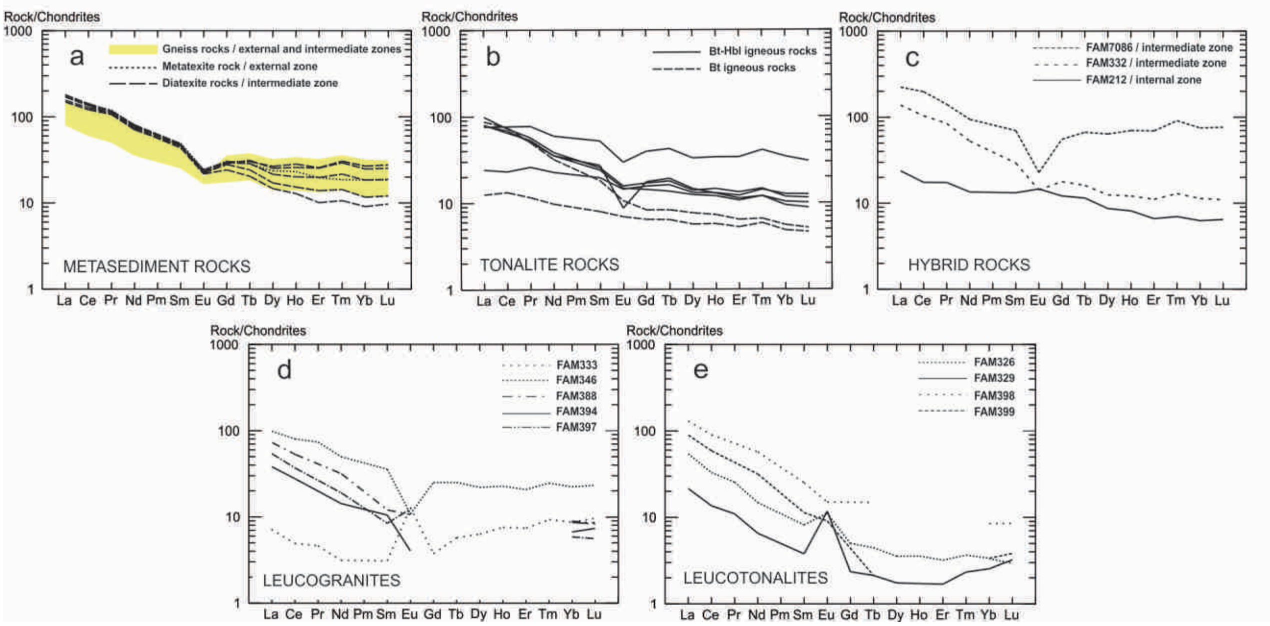

Figure 9. Alasino et al.

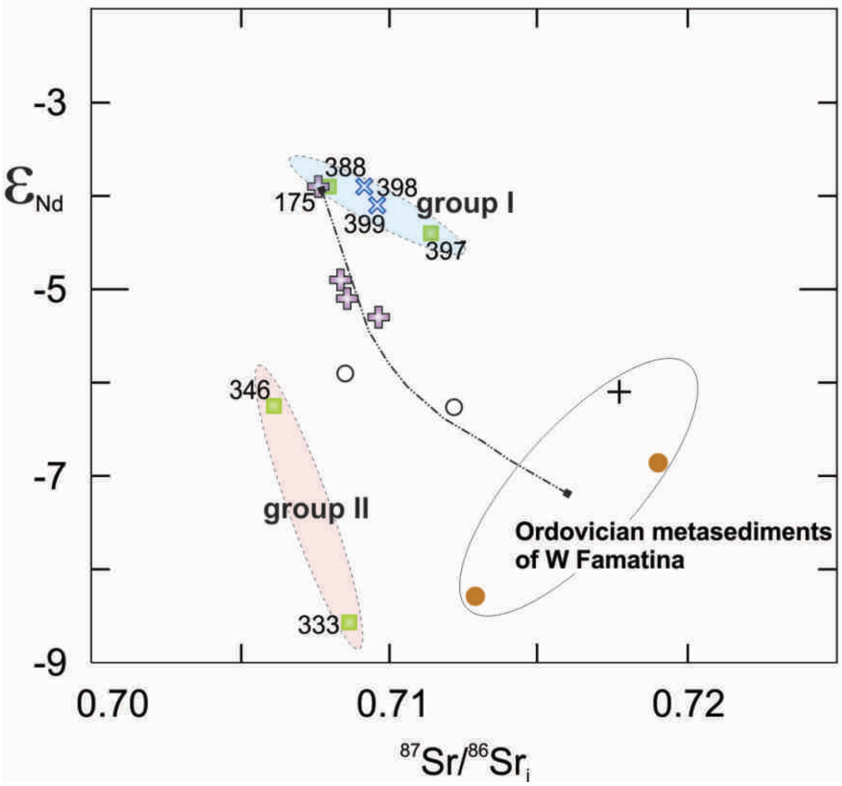

Figure 10. Alasino et al.

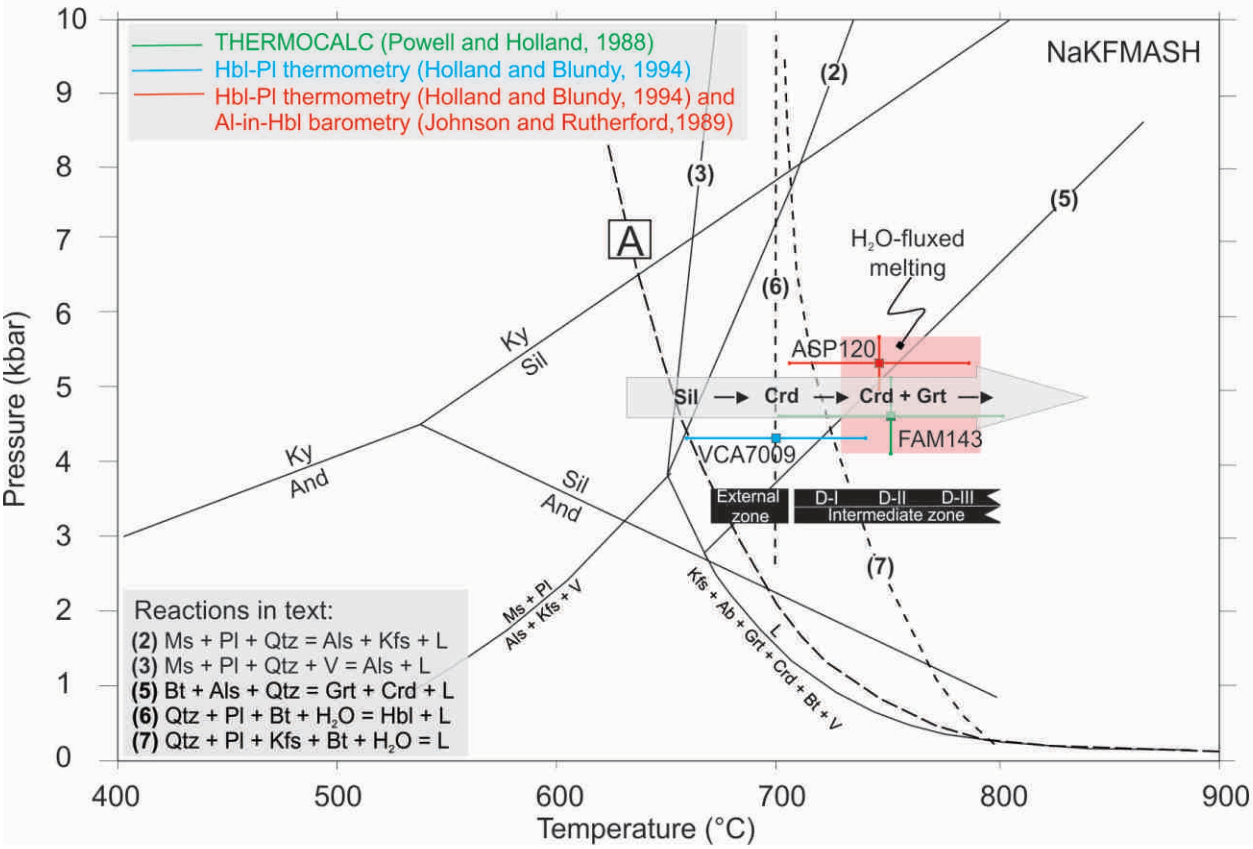

Figure 11. Alasino et al.

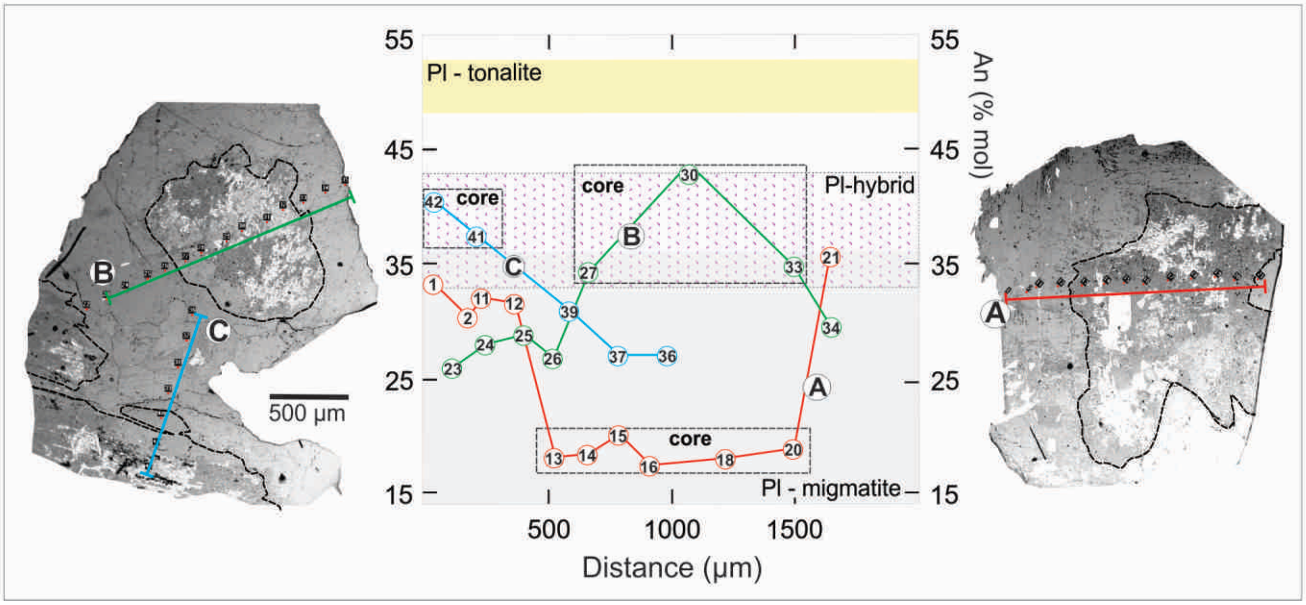

Figure 12. Alasino et al.

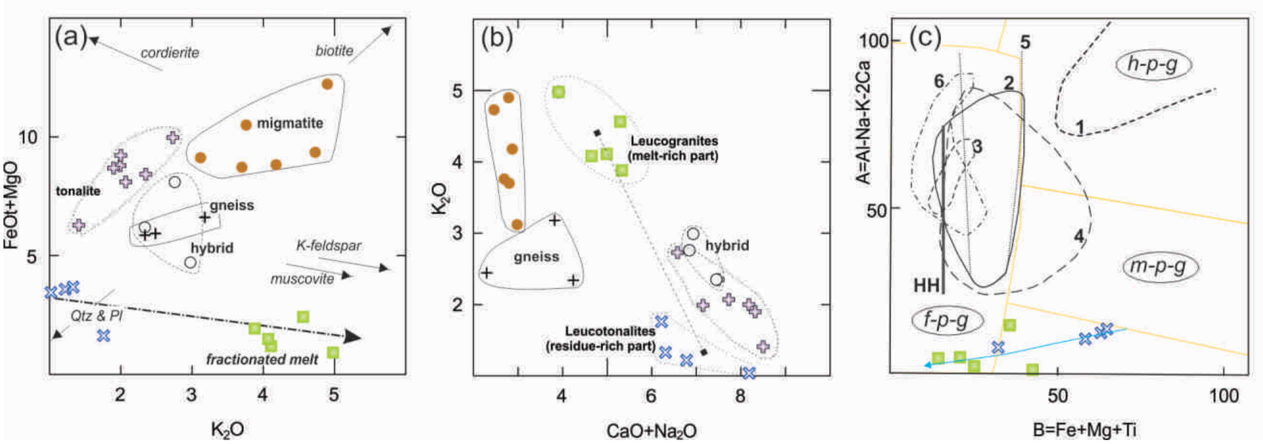

Figure 13. Alasino et al.

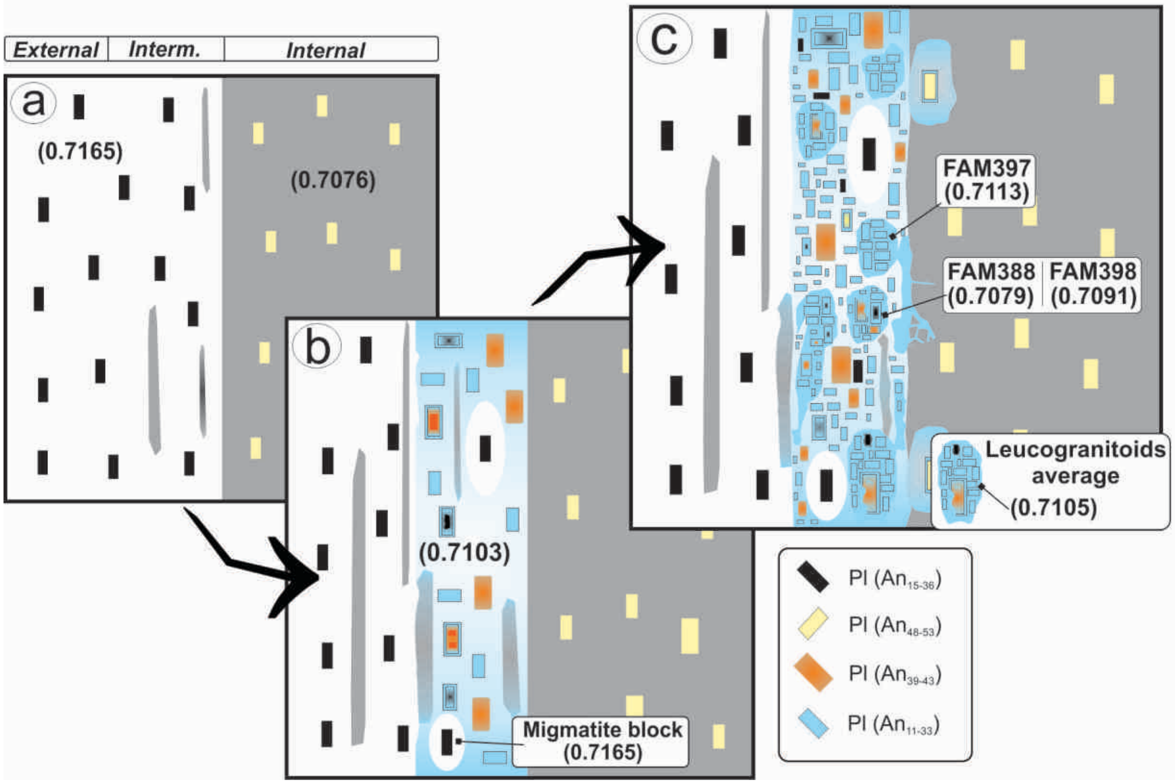

Figure 14. Alasino et al.

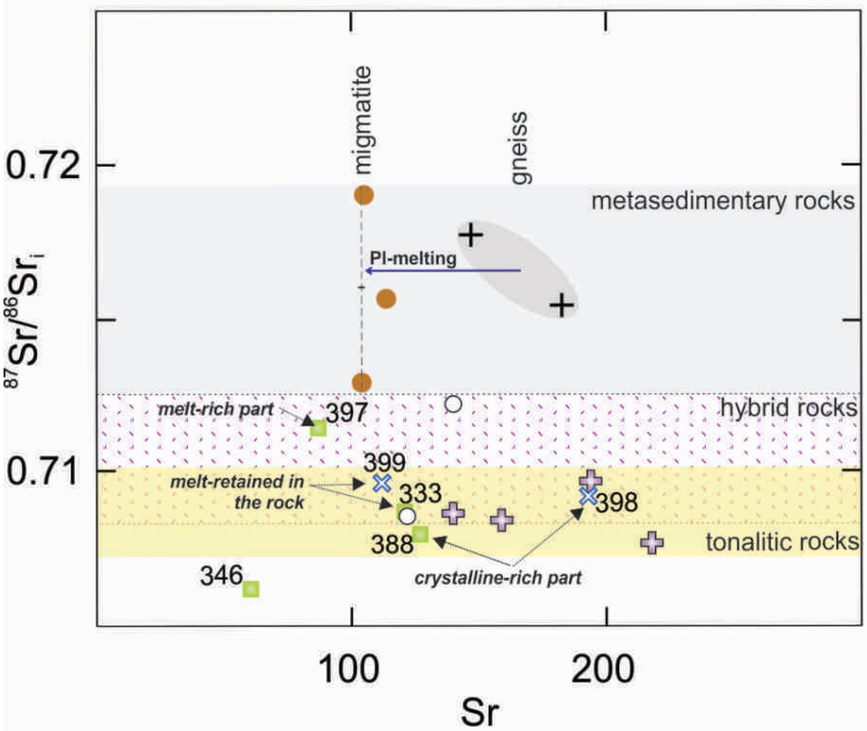

Figure 1. Simplified geological maps of NW Argentina: (a), Sierras Pampeanas; (b), Western Sierra de Famatina. Key for Fig. 1(a): F, Sierra de Famatina; V, Sierra de Velasco; SF, Sierra de Valle Fértil. In figure 1(b) from W to E the external, intermediate and internal zones. Limit between external and intermediate zones is not visible, as a reference to this take the Vinchina river. The intermediate and internal zone is limited by red dashed line, this corresponds to main intrusive contact. In the intermediate zone, the domains I (D-I), II (D-II) and III (D-III) are based on the predominance of specific rock-types: D-I, Bt-Sill±Crd migmatite blocks; D-II, Bt-Sill±Grt±Crd migmatite blocks; and D-III, Bt±Amp±Cpx±Kfs hybrid rocks. PRP Peñón Rosado pluton. Sample FAM175 is outside the mapped area (see Supplementary data).

Figure 2. Field photographs (a) migmatite rocks from external zone; (b) common texture of leucogranitoids of the intermediate zone; (c) euhedral cordierite (note that it overprints the migmatitic foliation) in migmatites of the intermediate zone; (d) garnet crystals in a homogenous diatexite of the domain II, intermediate zone.

Figure 3. Intermediate zone: (a) migmatitic blocks of domains I (Crd-bearing) and II (Crd-Grt-bearing) surrounded by leucogranitoid sheeted bodies; (b) dismembering of an amphibolite layer leading to many stoped blocks within leucogranitic magma, partly concordant with the regional structure of the aureole; (c) mingling between the tonalitic unit and leucogranitoids; (d) gradual transition of hybrids to leucogranitoids without signs of retrogression; (e) gradual transition of tonalite and hybrid sheets, the latter containing mafic enclaves; (f) leucogranitoid intruding tonalite at the main intrusive contact (i.e., the boundary between intermediate and internal zones).

Figure 4. Diagram illustrating the sequence of processes that we infer for the generation of the rocks in the Cerro Toro aureole.

Figure 5. (a) Euhedral cordierite encloses foliation-forming biotite and fibrolite in a diatexite block of the domain-II, intermediate zone. (b) Hybrid rocks in the intermediate zone showing skeletal plagioclase core surrounded by more albitic rim. (c) Amphibole with rounded inclusions of quartz and plagioclase in a hybrid of the intermediate zone. (d) Monomineralic plagioclase domain in a Bt-leucotonalite of the intermediate zone (specimen FAM398). (e) K-feldspar as interstitial crystals or filling cavities forming micro-veins in partially dissolved plagioclase (Bt-leucotonalite of the intermediate zone, sample FAM399). (f) Leucogranite (FAM397) showing genuine granite texture with euhedral Ab-rich plagioclase. (g) Twinned K-feldspar with unzoned plagioclase showing convex boundaries (sample FAM333). To the left, a partially dissolved pre-existing plagioclase crystal. (h) Titanite associated with K-feldspar in leucogranite (FAM397). (i) Corroded and partially dissolved pre-existing plagioclase contained in anatectic granitoids (sample FAM388). Photo width is 4 mm, except in (c) it is 8 mm. For more information, see text and Table 1.

Figure 6. The four main groups of biotite recognized in the Cerro Toro aureole based on textural (a) and chemical (b) criteria. Type 1, metamorphic biotite; Type 2, partially decomposed or re-equilibrated type 1 biotite; Type 3, magmatic biotite hosted in leucogranitic magmas; Type 4, magmatic biotite belonging to the tonalitic unit. In (a) black corresponds to opaque minerals. In (b) the numbers in boxes correspond to those of analysed samples. For more information, see Table 1 and supplementary data.

Figure 7. Whole-rock major and trace element abundances of the Cerro Toro aureole (western Famatina). Mg-number [100*MgO/(MgO+FeO*) molar]. ASI [$Al_2O_3/(Na_2O+K_2O+CaO)$ molar]. K_2O vs SiO_2 diagram with classification boundaries after Le Maitre et al. (1989). For more information, see Table 1.

Figure 8. Chondrite-normalised (after Nakamura, 1974) REE plots of metamorphic and igneous rocks of the Cerro Toro aureole. For more information, see Table 1.

Figure 9. εNd vs. $^{87}Sr/^{86}Sr$ initial plot of metamorphic and igneous rocks from the Cerro Toro aureole. Symbols as in figure 7. Four samples (three tonalites = VCA 7038, 7039, 7040 and one hybrid = FAM7086) are from Dahlquist and Galindo (2004). The grey dashed line is a hypothetical simple two-component mixing trajectory.

Figure 10. P-T projection showing thermobarometric results from migmatite (FAM143), amphibolite (VCA7009) and tonalite (ASP120). Metamorphic evolution of the metasedimentary rocks is well

explained by reactions 1 through 7 (see text). Reactions 1 and 4 were not included. Reactions 2, 3 and 5 in the NaKMASH system are from Spear et al. (1999). Reactions 6 and 7 are from Büsch (1974) and Peterson and Newton (1989), respectively. The Al_2SiO_5 triple point is from Pattison (1992). The grey arrow indicates nearly isobaric heating path from the external to the innermost intermediate zone of the Cerro Toro aureole.

Figure 11. Back-scattered electron (BSE) images showing the location of electron microprobe spots for plagioclase crystals contained in a leucogranite sample and their corresponding anorthite (An) profiles (A, B and C). An-content of plagioclases from tonalite, hybrid (intermediate zone) and migmatite are also shown. For more information, see Table 1 and Supplementary data.

Figure 12. (a) K_2O versus FeO^t+MgO and (b) CaO+Na_2O versus K_2O diagrams showing metasedimentary rocks, hybrids, tonalites and leucogranitoids of the Cerro Toro aureole. In (a) the vectors for K-feldspar, muscovite, quartz + plagioclase and biotite also are shown. (c) A–B diagram after Debon and Le Fort (1983) and Villaseca et al. (1998), showing compositions of experimentally derived melts under water-absent and water-present partial melting at mid-crustal conditions [1, Vielzeuf and Holloway (1988); 2, Holtz and Johannes (1991); 3, Finger and Clemens (1995); 4, Montel and Vielzeuf (1997); 5, Patiño Douce and Johnston (1991); 5, Castro (2004)]. Natural series: HH High Himalaya (Vidal et al., 1982). Fields are: f-p-g (felsic peraluminous granitoids); h-p-g (highly peraluminous granitoids); m-p-g (moderately peraluminous granitoids); and l-p-g (low peraluminous granitoids). Symbols are as in figure 7.

Figure 13. Model for the formation of isotopic heterogeneities by crystal-melt separation from hybridization zone (after Beard, 2008). (a) Voluminous metaluminous magmas ($^{87}Sr/^{86}Sr$ = 0.7076) intruded as sheets into partially molten metasedimentary country-rocks ($^{87}Sr/^{86}Sr$ = 0.7165) under amphibolite facies conditions. (b) Extensive hybridization ($^{87}Sr/^{86}Sr$ = 0.7103) in the intermediate zone took place. Black and yellow rectangles represent antecrysts from metasedimentary rocks and tonalites (respectively). Antecrysts retain their isotopic features. New plagioclase (orange rectangle) partly composed of country-rock material and partly composed of I-type magmatic material is formed. (c) Variable crystal-melt separation from hybridization zone forming neocrysts (sky-blue rectangles) and crystal overgrowths (sky-blue rims). $^{87}Sr/^{86}Sr$ ratios will depend on the proportions of antecrysts and neocrystals. In the figure, numbers in parentheses without denomination of sample represent average of initial $^{87}Sr/^{86}Sr$ ratios from Table 4.

Figure 14. $^{87}Sr/^{86}Sr$ initial versus Sr content of metamorphic and igneous rocks from the Cerro Toro aureole. Four samples (three tonalites = VCA 7038, 7039, 7040 and one hybrid = FAM7086) were taken from Dahlquist and Galindo (2004). Symbols are as in figure 7.

Table 1. Summary of petrographic characteristics

General type rock Essential minerals	An% in plagioclase	Biotite type+	Accessory mineral
Regional gneisses			
quartz > plag > biotite	n.d	n.d	Opq, Fib and Ms*
Regional metatexites			
quartz > biotite > plag	14-15	type-1	Opq, Fib, Ap, Ms*
Diatexite blocks of the intermediate zone			
Domain I = quartz > plag > biotite > cordierite	15-36	type-1	Opq, Fib, Ap, Kfs, Ms*
Domain II = quartz > plag > biotite > cordierite > garnet	15-32	type-2	Opq, Fib, Ap, Kfs, Ms*
Regional tonalites			
plag > quartz > biotite > hornblende	48-53	type-4	Ep, Qpq, Kfs
Hybrid rocks of the intermediate zone			
plag > quartz > biotite	core 39-43; rim33	type-2	Ep, Opq, Mon, Zrn, Ms*, ±Amp, ±Cpx, ±Kfs, relic Opx
Hybrid rocks of the internal zone			
plag > quartz > biotite	core 39-45; rim 24-30	type-4	Bt, Hbl, Ep, Opq, Ap, ±Kfs
Leucogranite rocks of the intermediate zone			
quartz > K-feldspar > plag	11-25	types-2 and -3	Bt, Ep, Ttn, Ap, Ms*
Leucotonalite rocks of the intermediate zone			
plag > quartz > ±K-feldspar	17-42	type-2	Bt, Ep, Ttn, Ap, Opq, Ms*

Mineral abbreviations from Kretz (1983). plag = plagioclase. Ms* = secondary muscovite. +Types of biotite based on textural and chemical criteria (see text).

Table 2. Major and trace element concentrations of igneous and metamorphic rocks from the Cerro Toro aureole, W Sierra de Famatina.

	External zone								Intermediate zone				
Unit	Gg	Gg	Mg	To	To	To	To	To	Gg	Mg	Mg	Mg	Mg
Sample	FAM 391	VCA 1004	FAM 349	FAM 115	FAM 120	VCA 7038	VCA 7039	VCA 7040	FAM 203	FAM 135	FAM 143	FAM 145	FAM 339
SiO_2	71.77	74.96	59.25	62.94	61.13	62.71	62.67	60.52	71.33	64.65	60.72	63.31	65.8
TiO_2	0.76	0.77	1.17	0.65	0.68	0.61	0.71	0.93	0.76	0.56	0.79	0.89	0.78
Al_2O_3	11.92	10.93	19.40	15.57	15.69	16.22	15.88	16.1	13.62	15.82	17.53	16.01	17.89
FeO*	4.20	4.43	9.01	6.1	6.53	5.84	6.2	7.09	4.68	6.26	7.35	6.15	6.47
MnO	0.08	0.09	0.15	0.14	0.14	0.13	0.13	0.14	0.09	0.16	0.23	0.15	0.12
MgO	1.66	1.65	3.21	2.69	2.69	2.59	2.49	2.88	1.93	2.46	3.15	2.68	2.65
CaO	1.57	0.85	0.80	4.97	5.5	4.84	5.5	4.43	1.56	1.02	1.09	0.89	0.83
Na_2O	2.67	1.46	1.99	2.18	2.68	2.65	2.82	2.15	2.26	1.78	1.60	1.98	2.15
K_2O	2.34	2.48	4.90	1.99	2	2.35	1.9	2.73	3.18	3.70	3.76	4.18	3.12
P_2O_5	0.20	0.18	0.13	0.16	0.17	0.26	0.19	0.25	0.07	0.10	0.09	0.15	0.19
Total	97.17	97.80	100	97.39	97.21	98.2	98.49	97.22	99.48	96.51	96.31	96.39	100
ppm													
Cs	3.5	5.39	9.58	4.94	8.68	0.7	5.3	2.4	2.6	4.51	6.67	4.35	8.39
Rb	100	96	198	96.5	243	10	108	70	88	137	169	143	149
Sr	147	182	104	196	54.5	140	159	194	126	138	114	110	105
Ba	276	342	623	310	226	41	266	410	553	1180	565	493	403
La	38.9	26.29	56.6	32.6	26.5	4.13	28.8	26	49.8	59.0	59.8	56.2	49.2
Ce	77	51.8	118	62.9	56.3	11.5	64.8	59.5	106	123	121	117	104
Pr	nd	5.61	13.4	6.4	5.99	1.3	5.63	5.7	11.9	13.1	12.8	12.3	11.9
Nd	39	22.3	49.6	24.3	22.3	6.15	20.2	22.3	45.4	50.8	48.9	47.4	44.7
Sm	7.29	5.11	10.0	5.19	5.52	1.62	3.67	4.88	9.97	9.88	9.44	9.65	9.32
Eu	1.37	1.27	1.88	1.21	0.67	0.53	0.82	1.14	1.55	1.71	1.74	1.82	1.86
Gd	nd	4.88	8.42	4.68	4.85	1.78	2.29	3.95	9.84	7.72	7.93	8.11	8.3
Tb	1.1	0.86	1.34	0.84	0.9	0.3	0.39	0.64	1.78	1.14	1.47	1.35	1.42
Dy	nd	4.83	8.09	4.79	5	1.94	2.62	4.26	11.1	5.86	8.68	7.38	9.13
Ho	nd	0.98	1.62	1.02	0.9	0.4	0.51	0.84	2.39	1.07	1.81	1.41	1.98
Er	nd	2.97	4.43	2.99	2.54	1.18	1.44	2.41	7.29	3.13	5.71	4.45	5.78
Tm	nd	0.42	0.56	0.44	0.36	0.18	0.20	0.36	1.08	0.43	0.88	0.65	0.92
Yb	3.26	2.58	4.08	2.59	2.07	1.06	1.22	2.27	7.02	2.57	5.46	4.06	5.89
Lu	0.49	0.40	0.63	0.39	0.3	0.16	0.18	0.34	1.06	0.41	0.86	0.64	0.94
U	2.9	0.80	2.58	0.54	2.23	0.21	0.68	0.58	2.17	3.11	2.36	3.27	7.99
Th	11.7	5.36	20.4	6.87	12.3	0.89	9.37	5.53	23.4	20.5	19.2	17.9	17.7
Y	30	24.6	40.8	22.0	24.3	10.8	14.3	24.4	67.1	25.3	43.2	34.8	50.1
Nb	nd	10.5	20.3	9.65	16.9	2.9	8.9	9.2	11.1	10.6	15.7	18.1	15.5
Zr	392	154	238	147	87.1	25	130	163	294	202	211	247	155
Hf	9.8	4.5	6.62	4.48	3.17	0.8	3.2	3.9	8.2	6.5	6.45	7.77	4.57
Ta	< 0.3	0.55	1.24	0.52	1.56	0.08	0.55	0.46	0.81	0.88	1.03	1.28	1.25
#Mg	*41.3*	*39.9*	*38.8*	*44*	*42.3*	*44.1*	*41.7*	*42*	*42.4*	*41.2*	*43.3*	*43.7*	*42.2*
ASI	*1.28*	*1.76*	*2.00*	*1.08*	*0.97*	*1.08*	*0.98*	*1.15*	*1.39*	*1.85*	*2.07*	*1.77*	*2.24*

Major element oxides and trace elements were analysed by ACTLABS Canada and GeoAnalytical Lab (WSU), see text. nd: not determined. Gg, gneiss; Mg, migmatite; To, tonalite; Lgt, leucogranite; Lto, leucotonalite; Hy, hybrid; #Mg, magnesium number = 100*MgO/(MgO+FeO*) molar. ASI, aluminum saturation index = $Al_2O_3/(Na_2O+K_2O+CaO)$ molar.

Table 2. *Continuation*

	Intermediate zone											Internal zone	
Unit	Mg	Lgt	Lgt	Lgt	Lgt	Lgt	Lto	Lto	Lto	Lto	Hy	Hy	To
Sample	FAM 335	FAM 346	FAM 388	FAM 394	FAM 397	FAM 333	FAM 326	FAM 329	FAM 398	FAM 399	FAM 332	FAM 212	FAM 213
SiO_2	66.33	76.31	72.94	77.13	76.97	74.44	71.09	75.13	74.12	77.73	66.55	68.74	62.55
TiO_2	0.83	0.12	0.21	0.05	0.12	0.2	0.27	0.35	0.367	0.17	0.57	0.38	0.629
Al_2O_3	16.05	13.19	14.14	12.24	12.45	14.15	15.85	13.14	13.68	12.78	16.69	15.25	16.99
FeO*	6.32	0.97	1.87	0.87	1.32	1.42	2.82	2.83	2.68	1.08	4.63	3.56	5.85
MnO	0.17	0.05	0.04	0.02	0.03	0.05	0.08	0.05	0.03	0.02	0.09	0.08	0.13
MgO	3.03	0.22	0.52	0.05	0.14	0.51	0.63	0.85	0.9	0.55	1.52	1.11	2.25
CaO	0.93	1.63	2.64	0.84	1.54	2.2	3.88	3.41	2.29	1.14	4.19	3.91	5.38
Na_2O	1.53	3.36	2.66	3.07	3.11	3.13	4.31	2.9	4.49	5.08	3.26	3.02	2.35
K_2O	4.73	4.11	4.56	4.98	4.07	3.88	1.02	1.33	1.22	1.76	2.34	2.98	2.07
P_2O_5	0.07	0.04	0.06	0.01	0.02	0.03	0.04	0.02	0.05	0.02	0.17	0.10	0.16
Total	99.99	100	99.64	99.26	99.77	100	99.99	100	99.83	100.3	100	99.13	98.36
ppm													
Cs	2.86	2.33	1.4	0.7	1.4	7.58	1.87	4.61	1.3	0.8	6.87	4.5	6.3
Rb	120	157	90	170	90	119	41.1	69.4	40	50	122	111	112
Sr	119	60.5	127	15	87	121	171	145	193	112	140	164	217
Ba	867	340	555	30	695	445	121	97.1	267	166	241	605	406
La	51.5	32.5	24.1	12.6	17.9	2.37	17.9	7.11	43	29.5	7.85	45.6	7.99
Ce	110	69.4	46	24	32	4.29	28.5	11.8	78	51	15.1	89.9	20
Pr	12.4	8.26	nd	nd	nd	0.52	2.86	1.23	nd	nd	1.95	9.48	2.92
Nd	45.8	31.5	20	9	12	1.99	9.36	4.13	36	20	8.53	33.2	14.3
Sm	8.85	7.24	2.44	2.13	1.71	0.63	1.66	0.77	5.12	2.31	2.69	5.95	3.98
Eu	1.67	0.83	0.82	0.31	0.95	0.99	0.86	0.91	1.16	0.7	1.13	1.1	1.11
Gd	6.69	6.91	nd	nd	nd	1.04	1.38	0.65	nd	nd	3.35	4.91	4.32
Tb	0.96	1.18	< 0.1	< 0.1	< 0.1	0.27	0.21	0.1	0.7	0.1	0.54	0.76	0.76
Dy	5.03	7.55	nd	nd	nd	2.18	1.22	0.6	nd	nd	2.98	4.29	4.51
Ho	0.9	1.59	nd	nd	nd	0.53	0.25	0.12	nd	nd	0.57	0.85	0.91
Er	2.27	4.66	nd	nd	nd	1.67	0.72	0.38	nd	nd	1.49	2.5	2.74
Tm	0.32	0.74	nd	nd	nd	0.28	0.11	0.07	nd	nd	0.21	0.39	0.43
Yb	2	4.91	1.96	1.47	1.29	1.91	0.74	0.56	1.86	0.73	1.38	2.5	2.78
Lu	0.33	0.79	0.29	0.25	0.19	0.33	0.13	0.11	0.29	0.1	0.22	0.37	0.43
U	1.91	1.82	0.8	3.2	1	1.17	0.97	1.75	1.4	0.5	0.89	2.01	2.15
Th	29.9	18.2	3.9	21	5.1	1.97	2.07	1	10.1	2.7	1.62	17.6	1.47
Y	22.6	41.8	18	10	11	15.4	6.71	3.55	19	6	14.3	23.7	25
Nb	11.6	10.1	nd	nd	nd	4.38	8.08	8.77	nd	nd	15.4	8.8	7.7
Zr	222	84.2	97	71	118	115	123	96.3	202	108	208	125	167
Hf	6.45	3.25	3.5	3.8	3.2	3.91	3.7	3.29	5.4	4	5.38	3.7	4.5
Ta	0.93	0.6	< 0.3	< 0.3	0.6	0.83	0.31	0.83	< 0.3	0.9	1.6	0.83	0.72
#Mg	*46.1*	*28.8*	*1.01*	*1.02*	*1.01*	*39*	*28.5*	*34.9*	*37.4*	*47.6*	*36.9*	*35.7*	*40.7*
ASI	*1.75*	*1.03*	*1.40*	*0.70*	*1.4*	*1.07*	*1.05*	*1.06*	*1.07*	*1.04*	*1.11*	*1.01*	*1.10*

Table 3. Summary of thermobarometric results.

1. Sample VCA7009, an amphibolite of the Cerro Asperecito, external zone								
Holland and Blundy (1994)	(Ed-Tr) at 5kb	T = 694 ± 40 °C						
	(Ed-Tr) at 5kb	T = 700 ± 40 °C						
2. Sample FAM143, a Crd-Grt migmatite block of the domain-II, intermediate zone+								
Activities and their uncertainties		phl	ann	py	gr	alm	spss	an
	a	0.0194	0.0570	0.00200	4.90e-5	0.320	0.00220	0.430
	sd(a)/a	0.44450	0.34057	0.68750	0.83534	0.15000	0.68112	0.09747
		ab	crd	fcrd	mncrd	san	ab	
	a	0.670	0.330	0.190	0.000680	0.860	0.400	
	sd(a)/a	0.05000	0.13467	0.19093	14.70588	0.05000	0.10800	
	activity 1 = Sill, H_2O, Qtz							
Independent set of reactions	1) gr + 2sill + q = 3an							
	2) 2py + 4sill + 5q = 3crd							
	3) 2spss + 4sill + 5q = 3mncrd							
	4) 5ann + 6fcrd = 9alm + 5san + $5H_2O$ + 3sill							
	5) 5gr + 3fcrd + 6sill = 2alm + 15an							
	6) phl + 6an = py + 2gr + san + H_2O + 3sill							
Results	*T = 751 ºC, sd = 51,*							
	P = 4.6 kbars, sd = 0.7, cor = 0.833, sigfit = 0.61							
3. Sample ASP120, a tonalite of the Cerro Toro complex, external zone								
Holland and Blundy (1994)	Hbl-Pl	T = 746 ± 40 °C						
Johnson and Rutherford (1989)	Al-in-Hbl		*P = 5.3 ± 0.5 kbars*					
4. A tonalite of the Cerro Toro complex, intermediate zone*								
Johnson and Rutherford (1989)	Al-in-Hbl		*P = 5.4 ± 0.5 kbars*					

+THERMOCALC software (Powell & Holland, 1988) and the updated version of the ds55 thermodynamic data set (November, 2003; Holland & Powell, 1998). Activity calculated with AX software at 5 kbars and 750º C.
*Sample from Saavedra et al. (1996). For mineral chemistry see supplementary electronic data.

Table 4. Rb-Sr and Sm-Nd data for some metamorphic and igneous rocks of the Cerro Toro aureole, Western Sierra de Famatina.

	SiO_2	Age (Ma)	Rb	Sr	$^{86}Rb/^{87}Sr$	$(^{87}Sr/^{86}Sr)_{today}$	$(^{87}Sr/^{86}Sr)_t$	εSr(t)	Rock type
Metasedimentary rock									
FAM349	59.25	481	211	106	5.7955	0.752604	0.712885	127	Mg
FAM391	71.77	481	100	147	1.9727	0.731227	0.717707	196	Gg
FAM143	60.72	481	158	119	3.8619	0.74267	0.716202	174	Mg
FAM339	65.80	481	137	115	3.4491	0.742651	0.719012	214	Mg
Regional Tonalite, internal zone									
FAM175	66.50	481	58	235	0.7178	0.712539	0.707619	52	To
Hybrid of the intermediate zone									
FAM332	66.55	481	112	123	2.6405	0.730251	0.712154	117	To
Leucogranitoids of the intermediate zone									
FAM333	74.44	481	109	111	2.8546	0.728216	0.708651	67	Lgto
FAM346	76.31	481	150	56	7.7734	0.759402	0.706127	31	Lgto
FAM388	72.94	481	90	127	2.0532	0.722063	0.707991	58	Lgto
FAM394	77.13	481	170	15	33.6395	0.972454	0.741903	540	Lgto
FAM397	76.97	481	90	87	3.0001	0.731954	0.711392	106	Lgto
FAM398	74.12	481	40	193	0.6000	0.713272	0.709160	74	Lto
FAM399	77.73	481	50	112	1.2930	0.718453	0.709591	80	Lto

	SiO_2	Age (Ma)	Sm	Nd	$^{147}Sm/^{144}Nd$	$(^{143}Sm/^{144}Nd)_{today}$	$(^{147}Sm/^{144}Nd)_t$	εNd(t)	T_{DM}*(Ga)
Metasedimentary rock									
FAM349	59.25	481	10.01	49.66	0.1218	0.511978	0.511594	-8.3	1.83
FAM391	71.77	481	7.29	39	0.1130	0.512047	0.511691	-6.4	1.70
FAM339	65.80	481	9.32	44.68	0.1261	0.512064	0.511667	-6.9	1.73
Tonalite of the Internal zone									
FAM175	66.50	463	10.6	37.6	0.1704	0.512355	0.511818	-3.9	1.51
Hybrid of the Intermediate zone									
FAM332	66.55	481	2.69	8.53	0.1906	0.512298	0.511698	-6.3	1.69
Leucogranitoids of the Intermediate zone									
FAM333	74.44	481	0.63	1.99	0.1914	0.512183	0.511580	-8.6	1.85
FAM346	76.31	481	7.24	31.46	0.1391	0.512137	0.511698	-6.2	1.69
FAM388	72.94	481	2.44	20	0.0737	0.512053	0.511821	-3.9	1.51
FAM394	77.13	481	2.13	9	0.1431	0.512236	0.511785	-4.6	1.56
FAM397	76.97	481	1.71	12	0.0861	0.512064	0.511792	-4.4	1.55
FAM398	74.12	481	5.12	36	0.0860	0.512088	0.511818	-3.9	1.51
FAM399	77.73	481	2.31	20	0.0698	0.512026	0.511806	-4.1	1.53

The decay constants used in the calculations are the values $\lambda^{87}Rb=1.42\times10^{-11}$ and $\lambda^{147}Sm=6.54\times10^{-12}$ $year^{-1}$ recommended by the IUGS Subcommision for Geochronology (Steiger and Jäger, 1977). Epsilon-Sr (εSr) values were calculated relative to a uniform reservoir present day: $(^{86}Rb/^{87}Sr)^{today}{}_{UR}=0.0827$; $(^{87}Sr/^{86}Sr)^{today}{}_{UR}=0.7045$. Epsilon-Nd (εNd) values were calculated relative to a chondrite present day: $(^{143}Nd/^{144}Nd)^{today}{}_{CHUR}=0.512638$; $(^{143}Sm/^{144}Nd)^{today}{}_{CHUR}=0.1967$. t=time used for the calculation of the isotopic initial ratios. TDM*=calculated according to De Paolo et al. (1991). For more information, see Supplementary data. Gg, gneiss; Mg, migmatite; Gt, granite; To, tonalite; Lgto, leucogranite; Lto, leucotonalite.

Table 5. Estimates of degrees of partial melting (F) in the Cerro Toro aureole.

	Source	Residue	F
FeO*	4.32	7.35	0.41
MgO	1.65	3.15	0.48
Nb	10.6	16.7	0.33
Sc	16.3	23	0.29
Zn	73	155	0.53
Zr	154	211	0.27
Co	11.8	19.6	0.40
Cr	57.4	91	0.37
			Average 0.38

$F = (C_r - C_o)/C_r$ where C_o is the concentration of an element in the source and C_r is the concentration the same element but in the residue. Source corresponds to gneisses samples (FAM391 and VCA1004) and the residue to FAM143. Concentrations in wt % for major elements and ppm for trace elements. Data used in the calculation are available in the Table 2.